Orbital-scale environmental and climatic changes recorded in a new ~200,000-year-long multiproxy sedimentary record from Padul, southern Iberian Peninsula

Jon Camuera [a,*], Gonzalo Jiménez-Moreno [a], María J. Ramos-Román [a], Antonio García-Alix [a], Jaime L. Toney [b], R. Scott Anderson [c], Francisco Jiménez-Espejo [d], Darrell Kaufman [c], Jordon Bright [e], Cole Webster [c], Yurena Yanes [f], José S. Carrión [g], Naohiko Ohkouchi [d], Hisami Suga [d], Masako Yamame [h], Yusuke Yokoyama [i], Francisca Martínez-Ruiz [j]

[a] Departamento de Estratigrafía y Paleontología, Universidad de Granada, Spain
[b] School of Geographical and Earth Sciences, University of Glasgow, UK
[c] School of Earth and Sustainability, Northern Arizona University, USA
[d] Department of Biogeochemistry, Japan Agency for Marine-Earth Science and Technology (JAMSTEC), Japan
[e] 7351 E. Speedway Blvd, 30C, Tucson, AZ, USA
[f] Department of Geology, University of Cincinnati, USA
[g] Departamento de Biología Vegetal, Facultad de Biología, Universidad de Murcia, Spain
[h] Institute for Space-Earth Environmental Research, Nagoya University, Japan
[i] Atmosphere and Ocean Research Institute, University of Tokyo, Kashiwanoha, Chiba, Japan
[j] Instituto Andaluz de Ciencias de la Tierra (IACT), Consejo Superior de Investigaciones Científicas-Universidad de Granada (CSIC-UGR), Granada, Spain

ARTICLE INFO

ABSTRACT

Padul is one of the few wetland sites in southern Europe and the Mediterranean region that exhibits an unusually large temporal span (>100 kyr) and continuous Quaternary sedimentary record. Previous core-based studies from Padul yielded paleoecological datasets (i.e., pollen and organic geochemistry), but with a poor age control that resulted in rather arbitrary climate inferences. Therefore, precise age control and a multidisciplinary approach is necessary to understand long-term regional environmental and climate change and the associated local response of the Padul wetland environment. Here we present a new long sediment record (Padul-15-05) from this wetland in the southern Iberian Peninsula with the aim of improving the age control of the sedimentary sequence and carrying out up-to-date high-resolution multiproxy analyses. In this study the age control is based on 61 AMS radiocarbon dates for the last ca. 50 kyr BP and on the extent of amino acid racemization (AAR) in mollusc shells extending back ~118 kyr BP. No numerical ages are available for the bottom part of the core but the sediment accumulation rates (SAR) and the cyclostratigraphic analysis of the multiproxy data suggest that the core preserves a continuous record of the last ~197 kyr (from late MIS 7 to present) with millennial-scale time resolution. Sedimentological (lithology, magnetic susceptibility, XRD, color), geochemical (XRF, TOC, C/N, % carbonate content) and paleontological (pollen, charophytes, gastropods) data show co-varying cyclical paleoenvironmental changes linked to orbital-scale climatic variability. Silicon, magnetic susceptibility (MS) and total organic carbon (TOC) data show periodicities between ~26.2−19.6 kyr linked to insolation, which is strongly dominated by precession cycles at this latitude. High values of Si and MS data have been related to high siliciclastic/detrital input from Sierra Nevada range during minima in insolation due to enhanced soil weathering/erosion during regional aridity and lower forest cover recorded by the arboreal pollen, which could also be favored by a minor biogenic productivity. In addition, warm climate conditions during maxima in insolation mostly resulted in negative precipitation/evapotranspiration balance and low lake levels, while cold glacial and stadial periods were mainly characterized by positive precipitation/evapotranspiration balance, and therefore, high lake levels. The improved chronology of the Padul sedimentary sequence along with a multiproxy study permitted us to better relate

* Corresponding author.
    E-mail address: jcamuera@ugr.es (J. Camuera).

environmental and vegetation changes to climatic events and to demonstrate how both local (i.e., lake level, sedimentation) and regional (i.e., vegetation) environments responded to orbital-scale climate changes.

1. Introduction

Climate during the Quaternary has oscillated between glacial and interglacial conditions in response to Earth's orbital cycles. Long paleoenvironmental records are necessary to investigate recurrent climatic or paleoenvironmental changes occurring with a certain periodicity (e.g., glacial-interglacial cycles). Over the last few decades, a significant effort has been made to understand climate and environmental variability during the Quaternary in southern Europe and the Mediterranean region. A handful of continuous long terrestrial sedimentary sequences recording more than 100 kyr have been studied in the Mediterranean region, including well-known sites such as Lago Grande di Monticchio (Italy; Watts et al., 1996; Allen et al., 1999, 2000), Ioannina lake (Greece; Tzedakis et al., 2002, 2003a), Tenaghi Philippon (Greece; Wijmstra, 1969; Tzedakis et al., 2003b, 2006; Pross et al., 2015), Lake Ohrid (Macedonia/Albania; Wagner et al., 2014, 2017; Francke et al., 2016), Lake Van (Turkey; Litt et al., 2014) and Yammoûneh (Lebanon; Develle et al., 2011). These studies, together with other high-resolution multiproxy studies in long marine sedimentary cores from the nearby Alboran Sea (Combourieu-Nebout et al., 2002; Martrat et al., 2004; Fletcher and Sánchez-Goñi, 2008), reveal the high sensitivity of this region for recording orbital and millennial-scale climate variability. These multiproxy studies offer a plethora of paleoclimate and paleoenvironmental data to assess ocean-atmosphere linkages and examine local, regional and global climate patterns. However, in the Iberian Peninsula a limited number of long (>100 kyr) and continuous terrestrial sedimentary records have been described, including Villarquemado (González-Sampériz et al., 2013; García-Prieto, 2015), Carihuela Cave (Fernández et al., 2007), Fuentillejo maar lake (Ortiz et al., 2013) and Padul (Florschütz et al., 1971; Nestares and Torres, 1998).

The Padul wetland in southern Iberian Peninsula (Fig. 1) is an indispensable site for understanding past glacial/interglacial climate variability in the Mediterranean region due to its sensitive location between temperate and humid climate to the north and the subtropical and arid climate to the south. The Padul wetland has one of the longest and most continuous sediment records of southern Europe, with more than 100 m of peat and lacustrine sediments deposited over the last ~1 Ma (Ortiz et al., 2004a, 2010). Previous palynological studies from the Padul wetland (Menéndez-Amor and Florschütz, 1962, 1964; Florschütz et al., 1971; Pons and Reille, 1988) revealed a climatically induced regional vegetation changes during the late Quaternary, although noticeable discrepancies in the interpretation of the pollen data due to age control uncertainties demands further investigation. Florschütz et al. (1971), based on pollen data, suggested that sediment from the Eemian interglacial (MIS 5e, ~115–130 kyr BP) was reached at 24 m depth and that sequence extended back to the Holsteinian interglacial (MIS 11, ~350–400 kyr BP) at the base of their core at 70 m depth. On the contrary, Pons and Reille (1988), with very similar pollen data, interpreted the base of their core at 24 m depth as representing the first Prewürm interstadial (i.e., MIS 5c), not showing any other interglacial period apart from the Holocene for the upper 24 m. These different correlations of the vegetation changes to climatic events are mostly a consequence of the poor chronologic control of the different sediment cores. In particular, Florschütz et al. (1971) used the age control of a nearby sediment core from Menéndez-Amor and Florschütz (1964) that was based on only 14 radiocarbon dates (with a maximum age of 54 kyr BP), assuming the same sediment accumulation rates for both cores. Using age information based only on radiocarbon dating, they tried to reconstruct the vegetation of the last ~400 kyr. With respect to the study from Pons and Reille (1988), the vegetation results and interpretation of the last ~ 100 kyr is based only on 17 radiocarbon dates with a maximum age of 29,300 ± 600 years BP. A more recent core retrieving a 100 m-long sedimentary sequence was taken in Padul in 1997 (Nestares and Torres, 1998), from which Ortiz et al. (2004a, 2010) studied the organic geochemistry and lithology. In this core, the age control for the upper part of the core was based only on 9 radiocarbon dates with a maximum age of 17,300 ± 500 years BP. The older part of the core was dated using a combination of AAR, U/Th and paleomagnetic information. However, the AAR dating was based on the D/L ratios of several amino acids from different locations of southern Spain and not from the specific Padul wetland Ortiz et al. (2004a, b). Moreover, the U/Th results used for the older ages have to be taken carefully due to the problematic behavior of the U-series in open peatland and lake systems as recently outlined by Sierralta et al. (2017). Finally, Ortiz et al. (2004a, b) did not provide the paleomagnetic results from the Padul record, so the boundary between the Matuyama and Brunhes magnetozones is difficult to identify. In addition, their results were interpreted as local paleoenvironmental and paleohydrological changes at moderate to low temporal resolution, and the lack of additional multiproxy data limited their interpretation and linkages to global climate changes.

Therefore, improving the age control using higher resolution (61 radiocarbon dates) updated dating methodologies (AMS radiocarbon dating, including compound-specific radiocarbon dating, and AAR dating based on gastropods from Padul) and increasing the resolution of multiproxy analyses (i.e., lithology/facies, mineralogy, inorganic/organic geochemistry, magnetic susceptibility, palynological analysis) from the Padul sedimentary sequence were necessary to solve previous inconsistencies, facilitating the investigation of the response of the environment to rapid events and allowing more accurate correlations between millennial-scale paleoenvironmental changes with orbital- and suborbital-scale climate variability. In addition, a principal component analysis involving different multiproxy datasets (i.e., inorganic and organic geochemistry and magnetic susceptibility) under a well-constrained chronology was still imperative in order to obtain more accurate lake level estimations.

In this study we present a high-resolution multiproxy record from a new ~43 m-long core, Padul-15-05, taken from the Padul wetland. This study complements a previously published high-resolution paleoenvironmental and paleoclimatic record of the uppermost 3.67 m Holocene section of the Padul-15-05 core (Ramos-Román et al., 2018a; b). This new core was studied with the goals of (1) generating a highly resolved and robust age control and (2) obtaining new paleoenvironmental information at higher sampling resolution, integrating up-to-date geological, biological and geochemical proxies that were lacking from previous studies.
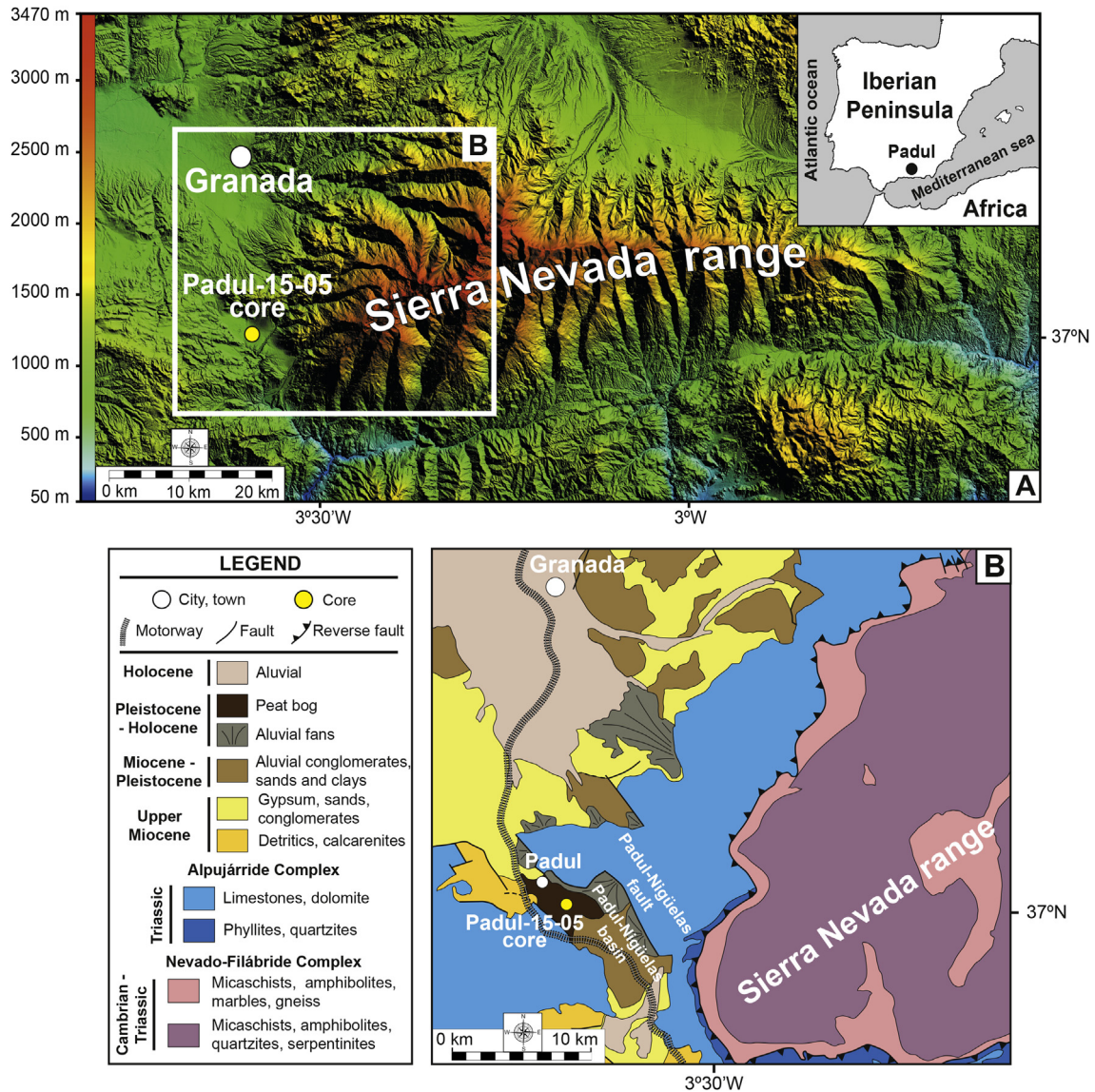
Fig. 1. (A) Geographical location of the Padul wetland in western Sierra Nevada range (southern Iberian Peninsula, western Mediterranean region) and the Padul-15-05 core, and (B) simplified geological map of the area surrounding Padul.

Here we also investigated (3) a detailed sedimentary facies analysis and its paleoenvironmental interpretation, which have been overlooked in previous studies. Finally, the new chronological and paleoenvironmental results presented here are (4) compared and discussed with respect to previous local and regional studies from Padul and the Mediterranean area and with insolation and ice volume records, sea surface temperatures from the western Mediterranean, and atmospheric temperatures from Greenland. This was done with the aim of understanding the environmental (i.e., lake levels, vegetation, sedimentation) response of this semiarid and climate sensitive region to orbital and suborbital climate variability.

2. Geographical and geological setting

2.1. Sierra Nevada range

The Padul wetland is located at the foothills of the Sierra Nevada range, which is an 85 km long and E-W aligned alpine mountain chain located in the Internal Zone of the Betic Cordillera (southern

Spain) (Fig. 1A). Elevation in Sierra Nevada ranges between ca. 900–3479 m a.s.l., including three of the five highest peaks on the Iberian Peninsula. Sierra Nevada was one of the southernmost European areas to be glaciated during cold phases of the Late Pleistocene (Schulte, 2002). Late Pleistocene valley glaciers occurred at higher elevation in Sierra Nevada than in other mountain ranges of the Iberian Peninsula due to its southernmost location and the nearby Mediterranean Sea influence (Gómez-Ortiz et al., 2005). Valley glaciers extended down to ca. 2300–2400 m on north-facing slopes and to ca. 2400–2500 m on south-facing slopes during the Late Pleistocene (Palacios et al., 2016). Erosion by Pleistocene valley and cirque glaciers allowed the formation of numerous small lakes and wetlands in high-elevation alpine environments after deglaciation (Castillo-Martín, 2009).

The Sierra Nevada range is formed by 3 main tectonic complexes according to different metamorphic facies: 1) Alpujárride, 2) Nevado-Filábride, and 3) Maláguide. Sierra Nevada is mainly formed by the Alpujárride Complex (mostly limestones and dolomites) and the Nevado-Filábride Complex (mostly mica schists), while the Maláguide Complex (mostly limestones and quartzites) is

restricted to a small area in the north of Sierra Nevada and NE of the city of Granada (Gonzalez-Donoso et al., 1978) (Fig. 1B).

2.2. Padul basin and wetland: geography, geology and climate

The Padul wetland is located 20 km south of Granada city (Andalusia, Spain) (Fig. 1B), in the western foothills of the Sierra Nevada and in the Internal Zone of Betic Cordillera. It occurs at 726 m a.s.l., in the NW-SE elongated Padul-Nigüelas extensional endorheic basin (12 km long, 4 km wide and total area of 45 km^2). This endorheic basin formed during the Alpine orogeny as a result of the extensional activity of the main Padul-Nigüelas normal fault, which is delimiting the NE edge of the basin with more than 250 m of vertical throw (Santanach et al., 1980), while the fault delineating the SW edge of the basin is antithetic to the Padul-Nigüelas fault and with less throw (Delgado et al., 2002). The different displacement of these two faults generated an asymmetric basin, causing deeper sedimentation and the formation of the Padul wetland at the NE edge of the basin (Domingo-García et al., 1983). Previous cores taken from the Padul wetland (Menéndez-Amor and Florschütz, 1964; Florschütz et al., 1971; Pons and Reille, 1988; Ortiz et al., 2004a) show different sediment thickness and sedimentation rates according to their proximity to the depocenter of the basin located nearby the main Padul-Nigüelas fault. Therefore, correlations with previous cores should not be done based on depth but with respect to lithology/facies and other proxy data (e.g., pollen). The Padul wetland likely exhibits a maximum sedimentary sequence depth greater than 100 m (Ortiz et al., 2004a). The presence of smaller faults in the basin that generated differential block subsidence could also result in different sedimentation thickness (Domingo-García et al., 1983).

The catchment of the Padul wetland comprises principally Triassic limestones and dolostones from the Alpujárride Complex and silicate-rich schists from the Nevado-Filábride Complex, whereas basin fill sediments are comprised of Upper Miocene conglomerates and calcarenites and Pliocene and Quaternary alluvial sediments and lacustrine deposits (González-Donoso et al., 1978; Domingo-García et al., 1983; Delgado et al., 2002). Therefore, the potential sedimentary input in the Padul-Nigüelas basin and in the Padul depression and wetland are Paleozoic-Triassic metamorphic and Triassic carbonate rocks eroded and carried by fluvial activity from the western side of Sierra Nevada and fluvial, alluvial, lacustrine and marine deposits from the Miocene and Pliocene basin fill (González-Donoso et al., 1978) (Fig. 1B).

This area is characterized by a semiarid Mediterranean climate (summer drought) with strong continental influence, with mean annual rainfall of 445 mm and mean annual temperature of 14.4 °C (agroclimap.aemet.es). The warmest month in Padul is July, with an average air temperature of 24.2 °C, whilst January is the coldest month, with temperatures averaging 6.4 °C. Most of the precipitation in this area occurs in December, averaging 68 mm (agroclimap.aemet.es). Due to its geographical situation, precipitation variability in this region is mostly controlled by the North Atlantic Oscillation, characterized by atmospheric pressure fluctuations between the Icelandic Low (cyclone) and Azores High (anticyclone) (Rodó et al., 1997; Lionello and Sanna, 2005). Groundwater flow from the aquifer of the dolomitic Trevenque Unit (one of the three units of the Alpujárride Complex described above) is the primary water source in the Padul wetland (Castillo Martín and Fernández-Rubio, 1984). Hydrogeological studies show that total water input is around 25 hm^3/yr, with 24 hm^3/yr corresponding to groundwater from the carbonate aquifer (Beas, 1990). Consequently, changes in the level of the water table in the Padul are directly controlled by water infiltration from the surrounding mountains into the aquifer, which occurs mainly during the snow melting season (Ortiz et al.,

2004a). The Padul wetland was drained for the first time in 1779 for agricultural purposes and more recently in 1943 for peat mining (Carrasco Duarte, 1998). The closure of one of the mines and the special environmental protection from the government since early 2000s allowed the regeneration and natural expansion of the wetland.

Local vegetation at Padul is mainly composed by wetland communities (Phragmites australis, Chara vulgaris …) while the regional vegetation is mainly composed of taxa belonging to mesomediterranean vegetation belt (Quercus rotundifolia, Q. faginea, Q. coccifera, Pistacia terebinthus, Celtis australis …). For further information about vegetation in Sierra Nevada range see El Aallali et al. (1998), Valle (2003) and Jiménez-Moreno et al. (2013), whereas for vegetation around Padul wetland see Pérez Raya and López Nieto (1991) and Ramos-Román et al. (2018a, b).

3. Materials and methods

3.1. Padul-15-05 core: drilling and sampling

The Padul-15-05 core was drilled at the present-day lakeshore during July 2015, 50 m from the current edge of the Padul wetland (37°00′39″N, 3°36′14″W). The continuous 42.64 m-long core was retrieved using a Rolatec RL-48-L hydraulic percussion coring machine from the Centre for Scientific Instrumentation of the University of Granada. Drilling ended at 42.64 m depth where the drill was unable to penetrate the hard lithology (conglomerates). The core was stored in a cooler at the Paleontology and Stratigraphy Department, University of Granada, where it was split into two halves and examined for lithology, and scanned for color analysis, continuous X-ray fluorescence (XRF) and magnetic susceptibility (MS). The core was sampled for different analyses, including accelerator mass spectrometry (AMS) radiocarbon dating, amino acid racemization (AAR) in molluscs, X-ray diffraction (XRD), organic geochemistry (Total Organic Carbon and C/N) and pollen analyses.

3.2. Dating and age-depth model

The age model for the Padul-15-05 core was developed using AMS-standard radiocarbon dating, specific compound radiocarbon dating on fatty acids, and by measuring the extent of AAR in mollusc shells (Fig. 2). The age for the lower part of the core, beyond where ^{14}C and AAR samples were taken, was constrained by extrapolating sedimentary rates from the ^{14}C-dated top part of the core as explained below (Fig. 2).

A total of 61 samples from different depths were analyzed for AMS radiocarbon dating, including plant remains (30 samples), organic bulk sediment (20 samples), pollen residues (5 samples), gastropod shells (3 samples) and specific compounds (3 samples) (Tables 1 and 2). Bulk sediment samples and pollen residues were used for dating due to absence of plant remains at some depths. All samples were dried and weighed before submission. Pollen residue samples were previously treated with hydrochloric acid (HCl) and hydrofluoric acid (HF) with the purpose of separating the organic material from detritals in the sediments.

Compound-specific radiocarbon analysis was conducted using the protocols of Yamane et al. (2014). Briefly, the sediment was extracted using dichloromethane/methanol (CH_2 Cl_2/MeOH, 7:3, v/v), and the total extract was saponified with KOH/MeOH. After removal of neutral components, the saponified solution was acidified with HCl and extracted with CH_2 Cl_2. This fraction was then esterified with HCl/MeOH. Separation of the fatty acid methyl esters (FAMEs) was conducted by silica gel column chromatography with/n/-hexane/CH_2 Cl_2 (2:1, v/v). Isolation of individual (C_16
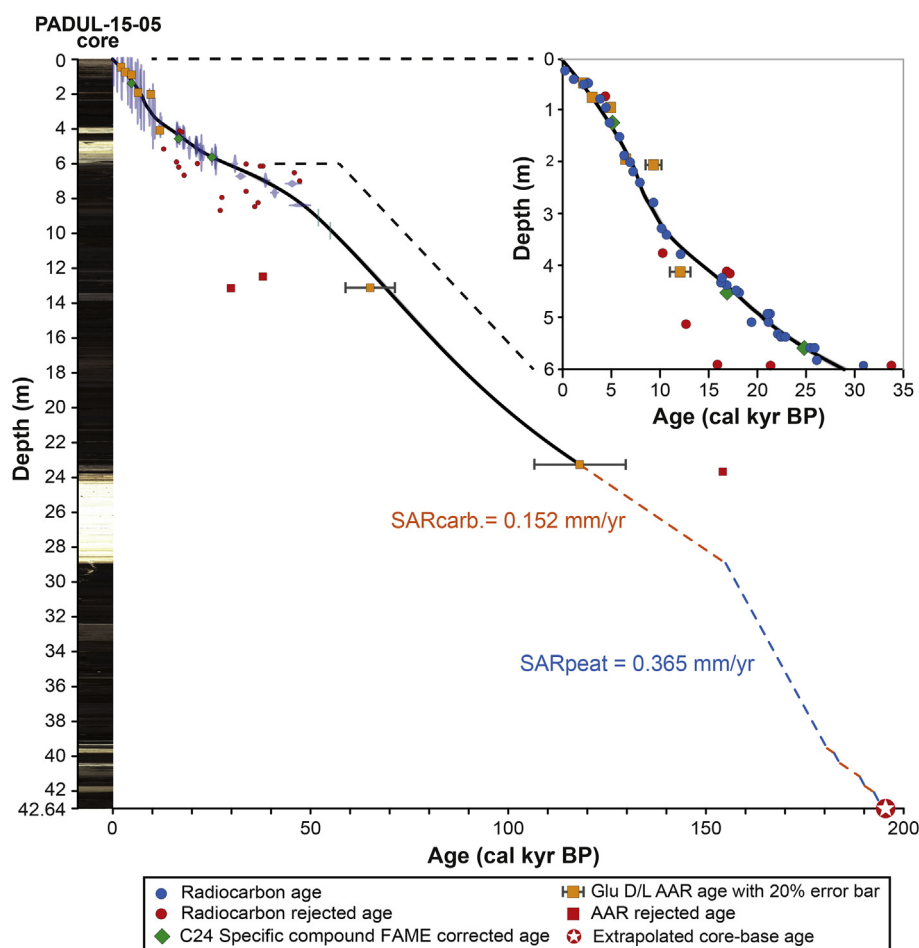
Fig. 2. Scanner photograph of the Padul-15-05 core along with the age-depth model. Sedimentary accumulation rates for peat and carbonate/marl lithologies (SARpeat and SARcarb, respectively) are marked. The right panel shows the detailed age-depth model of the top 6 m of the core.

−C_30) FAMEs was conducted using reversed-phase high-performance liquid chromatography (HPLC), with (Develosil C30-UG-5, 4.6 ′250 mm, 5.5 mm particle size). The mobile phase was MeCN/MeOH (1:2, v/v) with 0.5% pyridine. The column temperature was increased in steps of 15 °C from 0 to 35 min, ramped up at 2 °C/min from 35 to 52.5 min and finally held at 50 °C. The HPLC system consists of a binary pump, on-line degasser, autosampler, temperature controller (Polaratherm Series 9000), evaporative light scattering detector (ELSD; Polymer Laboratories PL-ELS 2100), and fraction collector. The flow rate of the mobile phase was 1 mL/min. The isolated fraction was then subjected to silica gel column to remove impurities. After the isolated FAMEs were collected and converted to graphite, radiocarbon measurement was conducted at the accelerator mass spectrometry facility at the University of Tokyo (Yokoyama et al., 2010). All radiocarbon values were corrected for the contribution of methyl carbon obtained from MeOH ($D^{14}C = -991‰$) during the esterification by isotope mass balance.

For amino acid racemization (AAR) (Figs. 2 and 3; Table 3), molluscs were cleaned by brief sonication, then soaked in 3% H_2O_2 for 2 h, rinsed with purified H_2O, then air dried under laminar flow. Single individual shells were placed in separate sterilized, conical bottomed micro-reaction vials and dissolved in 7 μL of 6 M HCl. Vials were sealed under N_2 and heated at 110 °C for 22 h to recover the total hydrolysable amino acid population. Hydrolysate solutions were evaporated to dryness *in vacuo,* then rehydrated in 4 μL of 0.01 M HCl with 1.5 mM sodium azide. The chromatographic instrumentation and procedure used to separate amino acid

enantiomers is presented by Kaufman and Manley (1998). Briefly, derivatization using *o*-phthaldialdehyde together with the chiral thiol, N-isobutyryl-ʟ-cysteine yielded fluorescent diastereomeric derivatives of chiral primary amino acids. The derivatization was performed on-line prior to each injection using the auto-injector of an integrated Agilent HP1100 liquid chromatograph. Separation was by a reverse-phase column packed with a C_{18} stationary phase using a linear gradient of aqueous sodium acetate, methanol and acetonitrile. Detection was by fluorescence.

The age model for the upper part of the core, from surface to 24.93 m depth, was created with the R-code package "Clam 2.2" (Blaauw, 2010), using the IntCal13.14C calibration curve (Reimer et al., 2013) and locally weighted spline age-depth model at 95% confidence range. For the lower part of the core, from 24.93 m to 42.64 m depth, the age model was created using linear extrapolation with two different sediment accumulation rates (SAR) calculated on the average peat and carbonate/marl lithology from the top part of the core.

3.3. Lithology and color

Lithology for the Padul-15-05 core was described in the laboratory of Paleontology and Stratigraphy at the University of Granada. The core was scanned for high-resolution photography and color data using the Avaatech core scanner from the CORELAB laboratory at the University of Barcelona (Spain). Numerical color results, such as lightness, RGB and CIELAB color space (b*) were

Table 1

AMS-standard radiocarbon ages from the Padul-15-05 sedimentary record (^{14}C ages for specific compounds have been included separately in Table 2). All radiocarbon ages were calibrated using R-code package "Clam 2.2" IntCal13.14C calibration curve at 95% confidence range. Rejected samples are marked in red.

	Material	Depth (cm)	δ^{13}C (‰)	Age (^{14}C yr BP ± 1σ)	Calibrated age (cal yr BP) 95% confidence interval	Median age (cal yr BP)
Reference age		0		2015 CE	-65	-65
D-AMS 008531	Plant remains	21,67	-11,3	103 ± 24	23 - 264	127
Poz-77568	Org. bulk sed.	38,46	-31	1205 ± 30	1014 - 1239	1130
BETA-437233	Plant remains	46,04	-24,3	2480 ± 30	2385 - 2722	2577
Poz-77569	Org. bulk sed.	48,21	-29,2	2255 ± 30	2158 - 2344	2251
BETA-415830	Gastropods	71,36	-10,1	3910 ± 30	4248 - 4421	4343
BETA- 437234	Plant remains	76,34	-28	3550 ± 30	3722 - 3956	3838
BETA-415831	Org. bulk sed.	92,94	-26,7	3960 ± 30	4297 - 4519	4431
Poz-74344	Plant remains	122,96	-26,4	4295 ± 35	4827 - 4959	4871
BETA-415832	Plant remains	150,04	-26,8	5050 ± 30	5728 - 5900	5814
Poz-77571	Plant remains	186,08	-29,2	5530 ± 40	6281 - 6402	6341
Poz-74345	Plant remains	199,33	-29,7	6080 ± 40	6797 - 7154	6935
BETA-415833	Org. bulk sed.	217,36	-26,8	6270 ± 30	7162 - 7262	7212
Poz-77572	Org. bulk sed.	238,68	-29,6	7080 ± 50	7797 - 7999	7910
Poz-74347	Plant remains	277,24	-29,6	8290 ± 40	9138 - 9426	9293
BETA-415834	Plant remains	327,29	-26,4	8960 ± 30	9932 - 10221	10107
Poz-77573	Plant remains	340,04	-29,8	9420 ± 50	10514 - 10766	10640
Poz-74348	Plant remains	375,62	-26,7	9120 ± 50	10199 - 10412	10305
Poz-79815	Org. bulk sed.	377,83	-28,6	10310 ± 50	11847 - 12388	12144
Poz-79817	Gastropods	411,02	-7,2	13910 ± 60	16588 - 17088	16838
Poz-79818	Gastropods	414,89	-6,8	14130 ± 50	17001 - 17419	17210
Poz-77574	Org. bulk sed.	423,65	-27,2	13580 ± 80	16113 - 16654	16384
Poz-79819	Org. bulk sed.	432,82	-31,3	13500 ± 60	16047 - 16494	16270
Poz-19821	Org. bulk sed.	437,92	-29,7	13910 ± 70	16570 - 17113	16841
Poz-79822	Org. bulk sed.	448,12	-29,7	14640 ± 70	17618 - 18011	17814
Poz-77575	Org. bulk sed.	452,2	-28,6	14890 ± 80	17898 - 18325	18111
Poz-79837	Org. bulk sed.	493,43	-28,7	17580 ± 80	20966 - 21527	21246
Poz-79838	Pollen residue	493,43	-32	17450 ± 80	20813 - 21352	21082
Poz-79839	Org. bulk sed.	509,26	-28,2	17510 ± 80	20885 - 21429	21157
Poz-79843	Pollen residue	509,26	-29,8	16060 ± 70	19173 - 19587	19380
Poz-74349	Plant remains (vertical roots)	513,22	-26,9	10740 ± 60	12582 - 12737	12659
Poz-79841	Pollen residue	532,24	-31,9	18210 ± 90	21836 - 22329	22082
Poz-77576	Org. bulk sed.	537,84	-27,5	19010 ± 120	22538 - 23255	22896
Poz-79842	Pollen residue	537,84	-26,5	18570 ± 80	22280 - 22628	22454
Poz-77820	Org. bulk sed.	559,25	-30,5	21650 ± 130	25691 - 26132	25911
Poz-79844	Pollen residue	559,76	-27,6	20790 ± 90	24660 - 25378	25019
BETA-437235	Plant remains	582,92	-15,7	21900 ± 80	25916 - 26331	26123
Poz-77577	Plant remains (vertical roots)	590,72	-29,8	13240 ± 70	15695 - 16142	15918
BETA-437236	Plant remains	598,52	-26,8	17650 ± 60	21075 - 21592	21333
Poz-77578	Org. bulk sed.	599,56	-31,9	26750 ± 240	30594 - 31221	30907
Poz-79845	Org. bulk sed.	601,64	-27,6	29930 ± 210	33678 - 34419	34048
Poz-79846	Org. bulk sed.	613,08	-26	33700 ± 310	37056 - 38796	37926
Poz-77579	Org. bulk sed.	614,12	-31,4	33400 ± 500	36400 - 38768	37584
Poz-74350	Plant remains (vertical roots)	617,76	-30,1	13680 ± 70	16254 - 16794	16524
Poz-77581	Org. bulk sed.	652,04	-29,5	43000 ± 1500	44397 - 49512	46954
BETA-437237	Plant remains	667,33	-25,5	14720 ± 50	17731 - 18075	17903
Poz-74351	Plant remains	672,94	-29,4	28550 ± 270	31700 - 33352	32526
BETA-437238	Plant remains	694,5	-27,4	34150 ± 200	38263 - 39106	38684
Poz-74352	Plant remains	701	-29,2	45000 ± 2000	45915 - 50000	47957
BETA-437239	Plant remains	714,5	-24,4	42030 ± 570	44453 - 46418	45435
BETA-415837	Plant remains	760,24	-27,1	29840 ± 160	33666 - 34240	33953
BETA-437240	Plant remains	765,96	-26,6	36300 ± 210	40434 - 41434	40934
Poz-74409	Plant remains	798,2	-29	23510 ± 130	27450 - 27861	27655
BETA-437241	Plant remains	826,28	-27,2	33000 ± 170	36461 - 37802	37131
Poz-74411	Plant remains	838,12	-29,1	44000 ± 1000	45675 - 49488	47581
BETA-437242	Plant remains	850,86	-27,6	32310 ± 180	35766 - 36604	36185
BETA-437243	Plant remains	871,25	-25,5	22820 ± 100	26908 - 27448	27178
Poz-74412	Plant remains	909,48	-29,7	> 52000		52000
Poz-74413	Plant remains	984,95	-27,4	> 55000		55000

Table 2
Age data from specific compound radiocarbon dating from Padul-15-05. Ages were calibrated using IntCal13.14C calibration curve at 95% confidence range. The selected C_{24} specific compound ages used for the age-depth model are marked in green.

Laboratory number (YAUT)	Depth (cm)	Specific compound	Sample amount (µgC)	Sample amount (µgC) (estimated by gas press.)	$\delta^{13}C$	$\Delta^{14}C$	pMC	^{14}C age (yr BP)	FAME corrected $\Delta^{14}C$	FAME corrected pMC	FAME corrected ^{14}C age (yr BP)	Age ranges (cal yr BP)	Median age (cal yr BP)
28335		C16 + C18	48	62,4	-37.7 ± 1.22	-458.28 ± 4.39	54.61 ± 0.44	4859 ± 65	-427.23 ± 4.64	57.74 ± 0.47	4411 ± 65	4854 - 5285	5017
28308	122,96	C20	201	196,1	-30.84 ± 3.90	-465.25 ± 3.92	53.91 ± 0.40	4963 ± 59	-440.78 ± 4.10	56.38 ± 0.41	4604 ± 59	5052 - 5570	5322
28334		C24	59	62,6	-25.92 ± 8.90	-448.33 ± 6.47	55.62 ± 0.65	4713 ± 94	-425.40 ± 6.74	57.93 ± 0.68	4386 ± 94	4826 - 5304	5008
28309		C26	185	151,2	-22.31 ± 3.48	-455.10 ± 4.15	54.93 ± 0.42	4812 ± 61	-435.74 ± 4.29	56.89 ± 0.43	4532 ± 61	4973 - 5443	5168
35722		C18	19	21,2	-32.38 ± 1.45	-739.79 ± 4.73	26.24 ± 0.48	10750 ± 145	-725.39 ± 4.99	27.69 ± 0.50	10315 ± 145	11410 - 12577	12112
35606		C20	166	152,8	-36.02 ± 2.54	-822.87 ± 1.39	17.86 ± 0.14	13840 ± 65	-814.06 ± 1.46	18.75 ± 0.15	13450 ± 65	15951 - 16419	16184
35615	452,2	C22	140	100,1	-40.82 ± 6.66	-820.35 ± 2.08	18.11 ± 0.21	13725 ± 95	-812.23 ± 2.17	18.93 ± 0.22	13370 ± 95	15780 - 16350	16085
35713		C23	37	34,5	-33.59 ± 1.08	-791.87 ± 2.79	20.98 ± 0.28	12540 ± 110	-782.87 ± 2.91	21.89 ± 0.29	12200 ± 110	13765 - 14620	14110
35614		C24	140	104,6	-38.37 ± 4.37	-832.09 ± 1.69	16.93 ± 0.17	14265 ± 80	-825.13 ± 1.76	17.63 ± 0.18	13940 ± 80	16579 - 17186	16905
35607		C26	167	144,0	-38.86 ± 2.92	-825.62 ± 1.42	17.58 ± 0.14	13965 ± 65	-818.95 ± 1.48	18.25 ± 0.15	13660 ± 65	16234 - 16756	16470
35719		C18	22	26,1	-23.15 ± 2.62	-876.08 ± 2.75	12.49 ± 0.28	16710 ± 180	-869.08 ± 2.90	13.18 ± 0.29	16275 ± 180	19171 - 20009	19647
35706		C20	44	61,4	-26.59 ± 0.55	-881.97 ± 1.54	11.90 ± 0.16	17100 ± 105	-876.12 ± 1.62	12.49 ± 0.16	16710 ± 105	19883 - 20467	20165
35707	559,25	C22	50	53,5	-34.91 ± 1.37	-896.37 ± 1.63	10.45 ± 0.16	18145 ± 125	-891.70 ± 1.70	10.92 ± 0.17	17790 ± 125	21140 - 21884	21541
35617		C24	103	107,9	-34.02 ± 3.90	-926.83 ± 1.00	7.38 ± 0.10	20940 ± 110	-923.82 ± 1.05	7.68 ± 0.11	20615 ± 110	24458 - 25206	24826
35618		C26	143	97,6	-42.51 ± 5.82	-907.00 ± 1.29	9.38 ± 0.13	19015 ± 110	-903.46 ± 1.34	9.73 ± 0.13	18715 ± 110	22370 - 22875	22581
35610		C28	130	117,9	-34.66 ± 3.88	-899.70 ± 1.09	10.11 ± 0.11	18405 ± 85	-896.16 ± 1.13	10.47 ± 0.11	18130 ± 85	21724 - 22269	21979
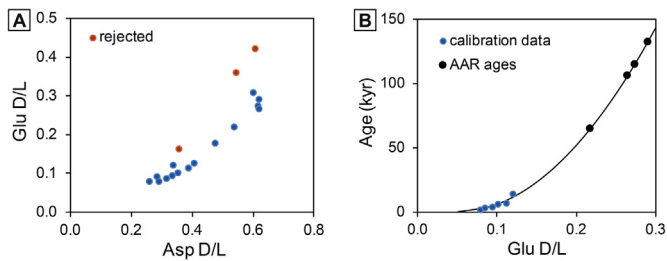
Fig. 3. Amino acid racemization results from the Padul-15-05 record. (A) Sample mean D/L values for aspartic acid (Asp) and glutamic acid (Glu); rejected samples fall of the trend defined by others. (B) Simple parabolic kinetic model fit through independently dates samples (blue circles) to estimate the ages of four gastropod samples (black circles). Data are listed in Table 3. (For interpretation of the references to color in this figure legend, the reader is referred to the Web version of this article.)

obtained (Fig. 4). Color data resolution was 0.073 mm so a resampling with a linear regular interpolation using the PAST 3.19 software (Hammer et al., 2001) was applied in order to obtain lower resolution results (0.5 mm resolution) comparable to other proxies.

3.4. Magnetic susceptibility

Magnetic susceptibility was measured to infer detrital input to the lake in relation with environmental and climate conditions. It was measured with a Bartington MS3 magnetic susceptibility meter operating with a MS2E sensor under stable temperature conditions in the Department of Stratigraphy and Paleontology, University of Granada (Spain). The maximum resolution of the MS3 meter was 2×10^{-6} SI and the operating frequency of the MS2E sensor was 2 kHz. Magnetic susceptibility was measured every 0.5 cm with a measuring time period of 10 s. Data are represented in Fig. 4.

3.5. Mineralogy

Thirty-six bulk sediment samples from different lithologies throughout the core were selected for X-ray diffraction (XRD) analyses in order to identify the mineralogical compositions of the different sedimentary facies and to provide accurate information about the relation between sedimentation, lake level and climate conditions. X-ray diffractograms were obtained using a PANalytical X'Pert PRO diffractometer with Cu-Kα radiation and automatic slit. Scans were run from 4° to 70° 2θ and semi-quantitative estimations of mineral abundance were obtained by using Xpowder software (Martin, 2004). The mineral components in the different facies are shown in Figs. 5 and 6 and Table 5.

3.6. Inorganic geochemistry

Inorganic geochemical composition of the sediments was obtained using a continuous XRF Avaatech core scanner from the CORELAB at the University of Barcelona (Spain). Measurements were taken at a resolution of 1 cm and under two different working conditions: (a) 10 s count time, 650µA of X-ray current and 10 kV of X-ray voltage for the measurement of Al, Si, P, S, Cl, Ar, K, Ca, Ti, V, Cr, Mn, Fe, Rh and Ag; and (b) 35 s count time, 1700µA of X-ray current and 30 kV of X-ray voltage for the measurement of Ni, Cu, Zn, Ga, Ge, As, Se, Br, Rb, Sr, Y, Zr, Nb, Au, Hg, Pb, Bi, Th and U. All results were expressed in counts per second (cps) and only values over 1000 counts were considered significant results. The most characteristic selected elements used as proxies for paleoenvironmental reconstruction (Al, Si, S, K, Ca, Fe, Br, Sr and Zr) have been represented in counts per second (cps) and as normalized data. Normalization was done dividing each element by the total counts including Si, K, Ca, Ti, Fe, Br, Sr and Zr. A Rb/Sr ratio was also calculated (Fig. 4). For the paleoclimate reconstruction of the entire Padul-15-05 record, non-normalized element data have been used due to their better correlation with other proxies (e.g., pollen) and providing better results in the statistical analyses (i.e., principal component analysis and spectral analysis, explained below).

3.7. Organic geochemistry

A total of 474 samples (mean sampling interval of ~37 cm from 42.64 m to 7 m depth and at ~2 cm resolution from 7 m depth to core top) were analyzed by means of a CHNS Elemental Analyzer Thermo Scientific Flash 2000 from the Centre for Scientific Instrumentation of the University of Granada (Spain). Samples were decalcified with 1:1 HCl before measuring. Atomic C/N ratio were calculated from the obtained TOC and TN (total nitrogen). TOC percentage was calculated from the percentage of carbon (%C) yielded by the elemental analyzer and recalculated by the weight of the sample before and after decalcification (also obtaining the total % of carbonate). Then, the organic matter (OM) in the sediment was

Table 3
Summary of amino acid racemization results from Padul-15-05. Rejected samples are marked in red.

UAL	depth (m)	n[a]	rej[b]	material	mean Asp D/L	stdev	mean Glu D/L	stdev	[14]C age (kyr)[c]	Glu D/L age (kyr)
14978	0,46	4	1	gastropod	0,292	0,024	0,079	0,011	2,0	2,1
15605	0,48	5	0	bivalve	0,261	0,009	0,079	0,003		
14979	0,75	3	2	gastropod	0,317	0,023	0,085	0,003	3,7	3,0
14980	0,92	4	0	gastropod	0,335	0,043	0,095	0,011	4,3	4,8
15606	0,92	3	1	bivalve - dirty	0,285	0,072	0,090	0,012		
14981	1,93	5	0	gastropod	0,354	0,032	0,102	0,008	6,6	6,4
14982	2,04	3	2	gastropod	0,388	0,037	0,113	0,008	6,9	9,3
15608	4,11	3	1	gastropod	0,339	0,054	0,121	0,009	14,3	11,8
15607	4,11	5	0	bivalve	0,406	0,013	0,127	0,010		
15444[d]	12,45	2	1	gastropod	0,477	0,055	0,178	0,031		38
15445	13,13	3	2	gastropod	0,538	0,032	0,218	0,017		65
15609[e]	13,13	5	0	bivalve - dirty	0,358	0,049	0,162	0,040		30
15446	22,98	4	1	gastropod	0,619	0,034	0,290	0,051		133
15447	23,37	4	1	gastropod	0,616	0,021	0,274	0,013		116
15448	23,42	4	1	gastropod	0,622	0,032	0,265	0,027		107
15611[e]	23,57	5	0	bivalve	0,543	0,050	0,359	0,043		222
15449[d]	23,57	2	1	gastropod	0,602	0,033	0,309	0,085		154
15610[e]	28,77	5	0	bivalve	0,608	0,009	0,421	0,020		320

[a] n = number of separate analyses used to calculate mean D/L, one individual per analysis
[b] rej = number of analyses rejected due to obvious signs of contamination by young amino acids
[c] independent age used to calibrate the rate of racemization
[d] sample rejected because too few individual analyses (n = 2)
[e] sample rejected because covarience between Asp D/L and Glu D/L falls off trend

estimated multiplying TOC by 1.724 of Van Bemmelen factor (Nelson and Sommers, 1982). Clay content in the samples is the remnant and could be calculated as follows (% Clay = 100 - % OM - % Carbonate). Data are represented in Fig. 9.

3.8. Palynological analysis

A total of 414 samples were analyzed for pollen analysis: 176 samples between 0 and 3.67 m (Ramos-Román et al., 2018b) and 238 samples between 3.67 and 42.64 m depth (Fig. 9). Pollen extraction followed a modified Faegri and Iversen (1989) methodology. *Lycopodium* spores were added to 1 cm³/sample of sediment for pollen concentration calculations. Hydrochloric acid (HCl), hydrofluoric acid (HF), sodium hydroxide (NaOH) and acetolysis were used to remove carbonates, silicates, humid acids, and cellulosic organic matter, respectively. The residue was sieved at 250 μm to remove very coarse vegetal and detrital remains prior to the NaOH and acetolysis treatments. Thereafter, the residue was sieved at 10 μm and subsequently mixed with glycerin for slide preparation and counting. A minimum of 300 terrestrial pollen grains per sample were identified using a Zeiss transmitted light microscope at 400 magnifications. A detailed pollen study and reconstruction of the vegetation is in preparation (Camuera et al. in prep.) and here we only show the abundance of Arboreal Pollen (AP) (sum of *Quercus* total, *Olea*, *Phillyrea*, *Fraxinus*, *Pistacia*, *Acer*, *Castanea*, *Corylus*, *Juglans*, *Betula*, *Alnus*, *Ulmus*, *Abies*, *Populus*, *Salix*, *Celtis*, *Carpinus*, *Cedrus*, *Taxus*, *Buxus*, *Tamarix*, *Hippophaë* and *Rhamnus*), which was calculated with respect to the total terrestrial pollen sum without *Pinus*, which is sometimes overrepresented.

Cyperaceae and *Typha* were not included in the total pollen sum, also because they are overrepresented in the local aquatic environment.

3.9. Principal component analysis (PCA)

PCA was run on the most representative inorganic geochemistry (Ca, Sr, Si, Al, Fe, S and Br), organic geochemistry (TOC and C/N) and magnetic susceptibility (MS) data using the PAST 3.19 software (Hammer et al., 2001) (Fig. 7). A previous resampling using linear interpolation was conducted to achieve equivalent resolution among different proxies. Moreover, all data were normalized using formula $X = (x - mean)/standard deviation$. Resampled and normalized data were further analyzed to determine the percentage of variance, scores, scatter plot and correlation loading plot. In addition to the PCA, a table with correlation coefficients was also computed as analytical approach (Table 4). Correlation coefficient was also calculated for Si (in counts per second) with respect to the Arboreal Pollen percentages, taking into account the specific depths that have been analyzed for the palynological analysis.

3.10. Spectral analysis

Spectral analysis using the REDFIT procedure of Schulz and Mudelsee (2002) was performed on Si, MS and TOC in order to identify cyclical periodicities using the PAST 3.19 software. This analysis focused on frequencies below 0.00025 (4000 years) for a better identification of the highest amplitude orbital-scale cycles (Fig. 8).
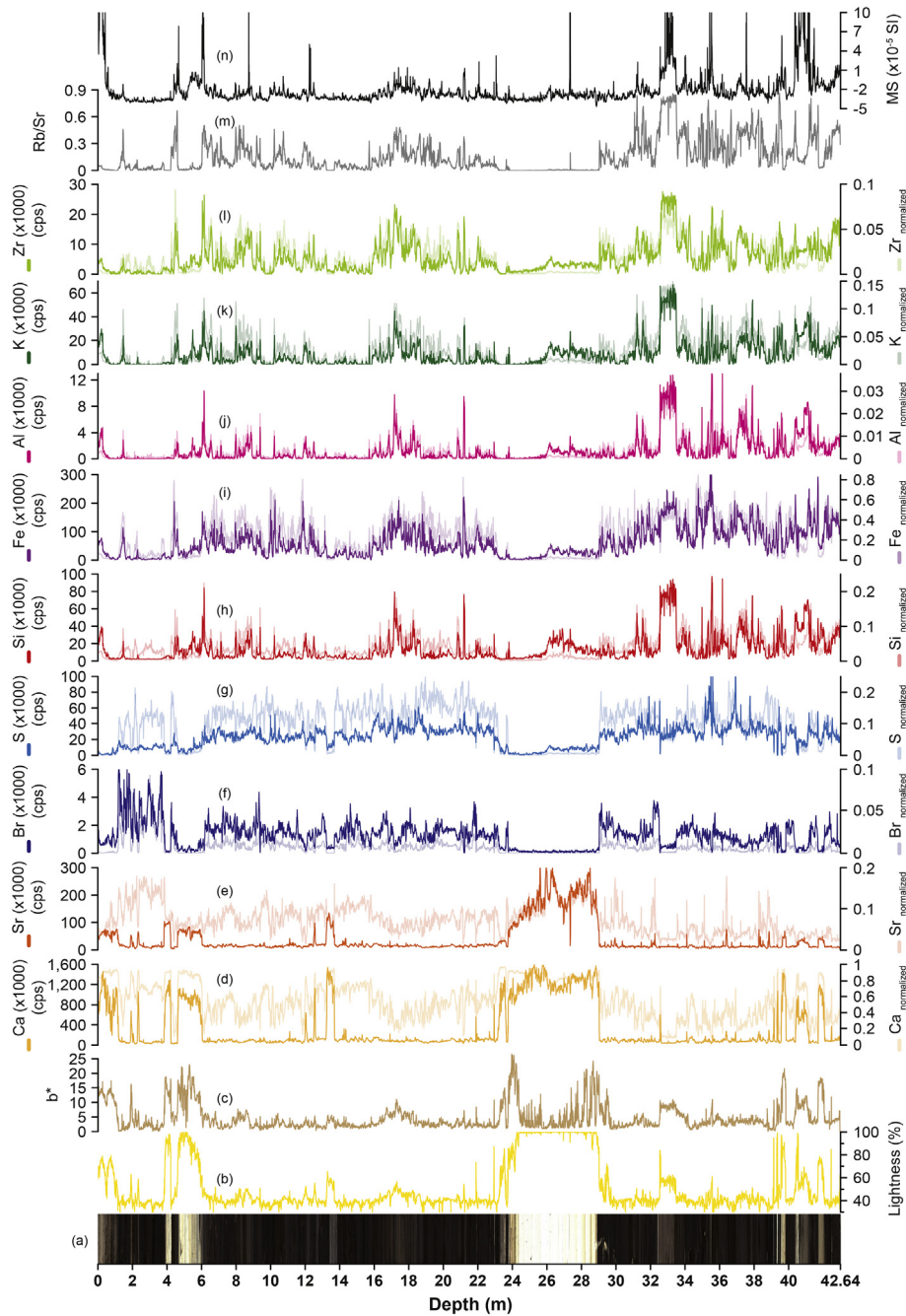
Fig. 4. Padul-15-05 core photo and physical and chemical data. From bottom to top: (a) scanner photograph of Padul-15-05 core, (b) lightness, (c) b* values, (d) Ca, (e) Sr, (f) Br, (g) S, (h) Si, (i) Fe, (j) Al, (k) K, (l) Zr, (m) Rb/Sr ratio, and (n) magnetic susceptibility (MS). XRF data have been represented in cps (dark line) and normalized (light line).

4. Results

4.1. Chronology and sediment accumulation rates (SAR)

4.1.1. AMS-standard radiocarbon dating

From the total of 61 radiocarbon dates (including 3 specific compound dates), 19 were excluded for the age model due to: reservoir effect (3 gastropod samples), vertical macrophyte roots from upper layers (3 plant remain samples), and seemingly too young dates (8 samples from plant remains) and too old dates (4 samples from bulk organic sediment and 1 sample from plant remains). The age-depth model for the last ~30,000 cal yrs BP (~6 m depth) of the Padul-15-05 core is quite robust and only 7 out of 42

AMS radiocarbon samples (including specific compound dates) were rejected (Tables 1 and 2). The δ^{13}C values in the analyzed samples mainly ranged from −24 to −32‰ (Table 1), pointing into terrestrial plants that use the C3 photosynthetic pathway (Deines, 1980). As for the three radiocarbon dates on FAMEs (at 122.96 cm, 542.2 cm and 559.25 cm depth), the C_{24} fatty acid was chosen for the age model because it derives from emerged plants (Ficken et al., 2000) in the studied context (i.e., Juncaceae, *Phragmites* or *Typha*). These plants display an in-situ growth, avoiding external inputs in the wetland system from longer chain fatty acids (terrestrial input) from the catchment basin (Table 2).

Several AMS radiocarbon dates older than ~30,000 cal yrs BP were not used in the age model, in particular: 1 root sample (at
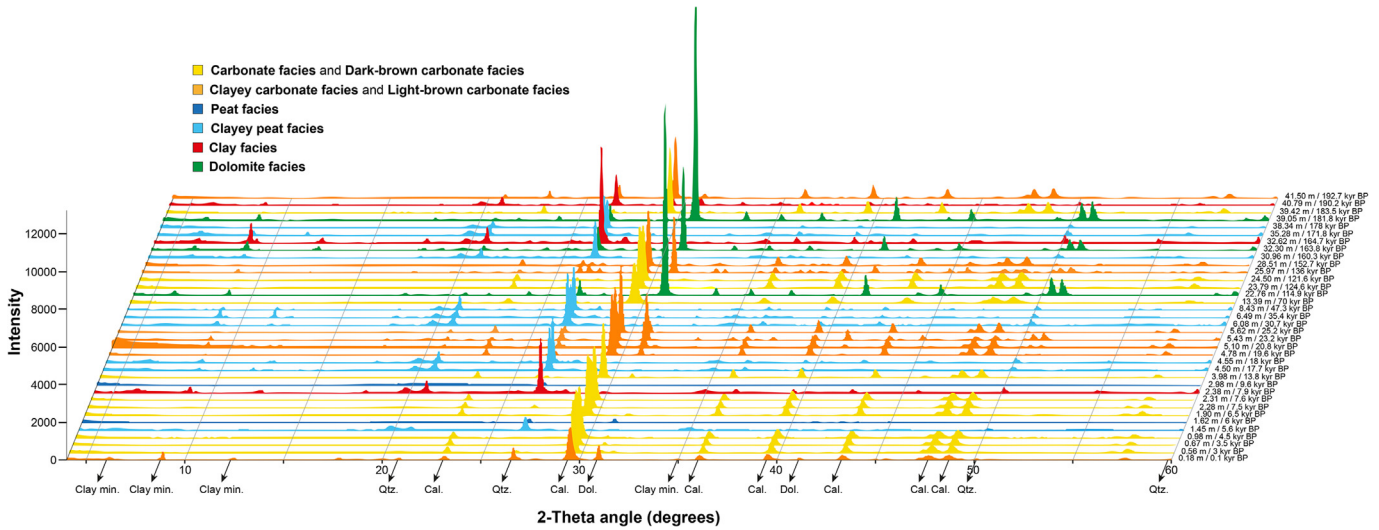
Fig. 5. All the studied diffractograms from Padul-15-05 colored according to their respective facies. Peaks from calcite, dolomite, quartz and clay minerals, as well as depth and age for every sample has been marked. The backgrounds from *Peat facies* samples have been deleted in order observe and compare all samples clearly (see the difference with respect to the original *Peat facies* diffractogram in Fig. 6). Note that *Carbonate facies* and *Dark-brown carbonate facies* have been represented in the same group because they present similar diffractograms, as also occur with *Clayey carbonate facies* and *Light-brown carbonate facies* (see Fig. 6). (For interpretation of the references to color in this figure legend, the reader is referred to the Web version of this article.)
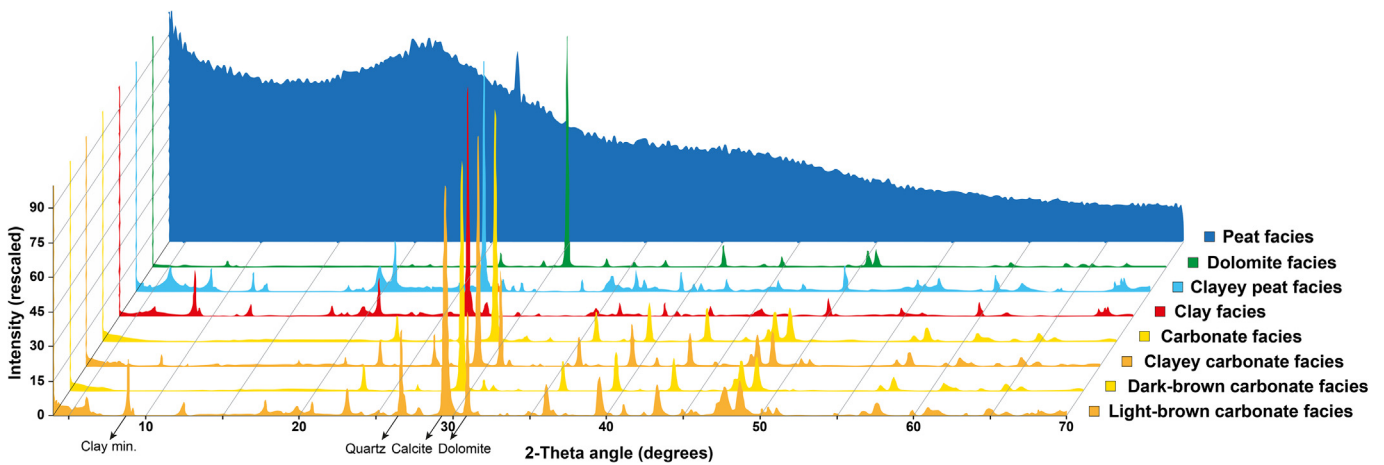
Fig. 6. Representation of the most characteristic diffractograms for every facies. The most representative peaks of clay minerals, quartz, calcite and dolomite have been marked.

Table 4
Correlation coefficients between the most representative XRF data (Ca, Sr, Si, Al, Fe, S, Br), magnetic susceptibility (MS), TOC and C/N from Padul-15-05. Positive correlations are marked in green while negative correlations are in red.

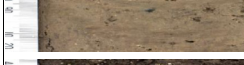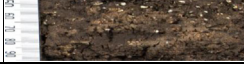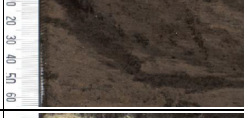|	Ca	Sr	Si	Al	MS	Fe	S	Br	TOC	C/N
Ca		0	1,9E-01	8,1E-11	3,1E-04	3,7E-174	0	0	0	3,9E-323
Sr	0,86		4,1E-02	7,5E-13	2E-05	1,1E-126	0	1,6E-278	0	1,1E-265
Si	-0,02	-0,03		0	6,9E-323	0	6,6E-16	2,8E-129	6,3E-115	2,8E-36
Al	-0,10	-0,11	0,98		2,8E-299	0	5,1E-25	2,9E-90	5,3E-69	5,0E-14
MS	0,06	-0,07	0,54	0,52		7,2E-144	9,6E-01	2,9E-47	2,3E-71	4,0E-40
Fe	-0,41	-0,35	0,65	0,66	0,38		0	1E-09	8,8E-01	1,7E-18
S	-0,66	-0,54	0,12	0,16	0,00	0,64		1,1E-54	4,8E-242	1,6E-267
Br	-0,61	-0,51	-0,36	-0,30	-0,22	-0,09	0,24		0	8,4E-48
TOC	-0,77	-0,65	-0,34	-0,27	-0,27	0,00	0,48	0,64		0
C/N	-0,54	-0,50	-0,19	-0,12	-0,20	0,13	0,50	0,22	0,72	
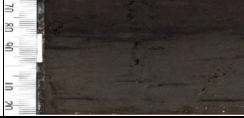
617.7 cm depth) that yielded a younger age probably contaminated from younger sediments, 4 organic bulk sediment samples (from 601.6 cm to 652 cm depth) too old with respect to previous/later ages and that would imply an excessively high SAR for the corresponding peat lithology, and 7 plant remain samples (from 667.3 cm to 871.2 cm depth) of which 6 yielded anomalously young ages interpreted as contamination from younger sediments.

Table 5
Schematic table showing a short description of the results and interpretations of different facies presented in the Padul-15-05 core. Relative values from different analyses have been colored for a better comprehension: very low (blue), low (green), medium (yellow), high (orange) and very high (red).

Facies	Core-scan images	Sedimentological features	Mineralogy	Most representative elemental/organic geochemistry and magnetic susceptibility		Depositional subenvironment	Relative lake level (0 to 5)
Peat facies		Black massive peat with high amount of organic matter and vegetal roots	Low quartz	Ca = 20,000 - 100,000 cps S = 10,000 - 75,000 cps TOC = 30 - 60 %	Si = 0 - 4,000 cps MS = < -3 x 10⁻⁵ SI C/N = 35 - 60	Very shallow palustrine environment with high amount of littoral vegetation and organic matter	1
Clayey peat facies		Organic clayey peat. Vegetal remains are common	Quartz, illite	Ca = 20,000 - 100,000 cps S = 10,000 - 75,000 cps TOC = 20 - 40 %	Si = 10,000 - 85,000 cps MS = < 3 x 10⁻⁵ SI C/N = 25 - 40	Shallow palustrine environment with detritic input from Sierra Nevada due to low forest cover during cold climate periods	1 - 2
Clayey carbonate facies		Yellowish carbonate with clayey layers. Frequent gastropods and pelecypods	Calcite, dolomite, low quartz	Ca = > 800,000 cps S = 5,000 - 25,000 cps TOC = 0 - 3 %	Si = 15,000 - 30,000 cps MS = < 1 x 10⁻⁵ SI C/N = 20 - 30	Opened high lake level stages. Clay/detritic input is related to cold periods with low forest cover	4 - 5
Carbonate facies		Light yellowish charophyte carbonate. Full of gastropods and pelecypods	Calcite	Ca = > 800,000 cps S = 0 - 6,000 cps TOC = 0 - 3 %	Si = 0 - 10,000 cps MS = < -2 x 10⁻⁵ SI C/N = 15 - 25	Opened high lake level phases that allowed the proliferation of organisms	4 - 5
Dark-brown carbonate facies and Light-brown carbonate facies		*Light-brown carbonate facies:* Light brown carbonate. Higher Si and MS than in *Dark-brown carbonate facies*	Calcite, dolomite quartz, illite	Ca = > 200,000 cps S = 0 - 8,000 cps	Si = 0 - 40,000 cps MS = -4 x 10⁻⁵ - 30 x 10⁻⁵ SI	*Light-brown carbonate facies:* Exposed lake stage with important detritic presence	0
		Dark-brown carbonate facies: Dark brown carbonate. Gastropods, pelecypods and charophytes more abundant	Calcite	TOC = 0 - 10 %	C/N = 0 - 25	*Dark-brown carbonate facies:* Shallow opened lake lake with proliferation of organisms	2 - 3
Clay facies		Brown clay organic bands. Presence of vegetal remains. Mottling and mixed sediment textures	Quartz, illite	Ca = 30,000 - 100,000 cps S = 20,000 - 45,000 cps TOC = 0 - 10 %	Si = 20,000 - 95,000 cps MS = -2 x 10⁻⁵ - 15 x 10⁻⁵ SI C/N = 15 - 30	Low water depth. Detritic input from Sierra Nevada is due to low forest cover linked to cold climate periods	1 - 2
Dolomite facies		Grayish white dolomitic cm-layers	Dolomite, low quartz	Ca = > 700,000 cps S = 0 - 5,000 cps TOC = 0 - 1 %	Si = 20,000 - 60,000 cps MS = < -1 x 10⁻⁵ SI C/N = 20 - 25	Episodes of high runoff during tectonic pulses and/or biogenically induced dolomite precipitation	1 - 2

* Values for every analysis are classified with colors as **Very low**, **Low**, **Medium**, **High** and **Very high** for a better comprehension.
Maximum values of the more relevant data from the PADUL-15-05 core: Ca = 1,600,000 cps, Si = 95,000 cps, S = 130,000 cps, MS = 40 x 10⁻⁵ SI; TOC = 60%, C/N = 60%

4.1.2. AAR dating

A total of 83 individual shells were analyzed separately for AAR dating from 14 levels in the core (Table 3), including gastropods (hydrobiid *Milesiana schuelei*) from 12 levels and pelecypods (*Pisidium* sp.) from 6 levels; both gastropods and pelecypods were analyzed from 4 levels. Five individual shells, each prepared separately, were analyzed from most levels. A total of 14 analyses (17%) were rejected because of obvious signs of contamination by young amino acids. The rejection rate was higher for gastropods than for pelecypods, which is common for AAR analyses.

Of the eight amino acids routinely separated by reverse phase HPLC, aspartic acid (Asp) and glutamic acid (Glu) are present in the highest concentrations (therefore better detected in the tiny specimens) and are resolved best by the chromatography (therefore highest precision). With few exceptions, D/L values increase down core (Table 3). The results for two of the gastropod samples (12.45 and 23.57 m depth) were rejected because they were based on only two individuals, which is insufficient to confidently determine a mean D/L value for the sample. The D/L values for one of the pelecypod samples (13.13 m depth) were unexpectedly low. Although a full suite of five individuals was analyzed for this sample, the result was rejected because the shells were heavily encrusted in carbonate and difficult to clean. For this sample and

two others (23.57 and 28.77 m depth), the covariance between D/L Asp and D/L Glu fell off of the expected trend as defined by the other samples and these were rejected (Fig. 3). Because the rate of racemization differs between pelecypods and gastropods, and because the AAR data from the three pelecypod samples beyond the range of ^{14}C dating were rejected, we focused on the results from the gastropods.

The rate of racemization (calibrated age equation) was quantified using the mean D/L values for six independently dated samples (^{14}C-based age-depth model), ranging in age from 2.0 to 14.3 kyr (Table 3). The rate of racemization was calibrated using a simple parabolic kinetic model (D/L = age$^{0.5}$) (Mitterer and Kriausakul, 1989). We focused on Glu because it has been shown to be well suited for older (middle Pleistocene) molluscs, whereas the apparent rate of racemization for Asp typically plateaus (e.g., Laabs and Kaufman, 2003).

Using least-squares regression to fit the sample-mean Glu D/L value to the square root of time yields the AAR age equation: $t = (1507.5 * D/L - 73.715)^2$, where t is age in years and D/L is the mean Glu D/L value for gastropods (Fig. 3). The parabolic function fits the D/L versus age data well ($r^2 = 0.89$, n = 6). No attempt was made to formally quantify the age uncertainty. At a minimum, the uncertainty includes the intra-sample variability in Glu D/L values, which
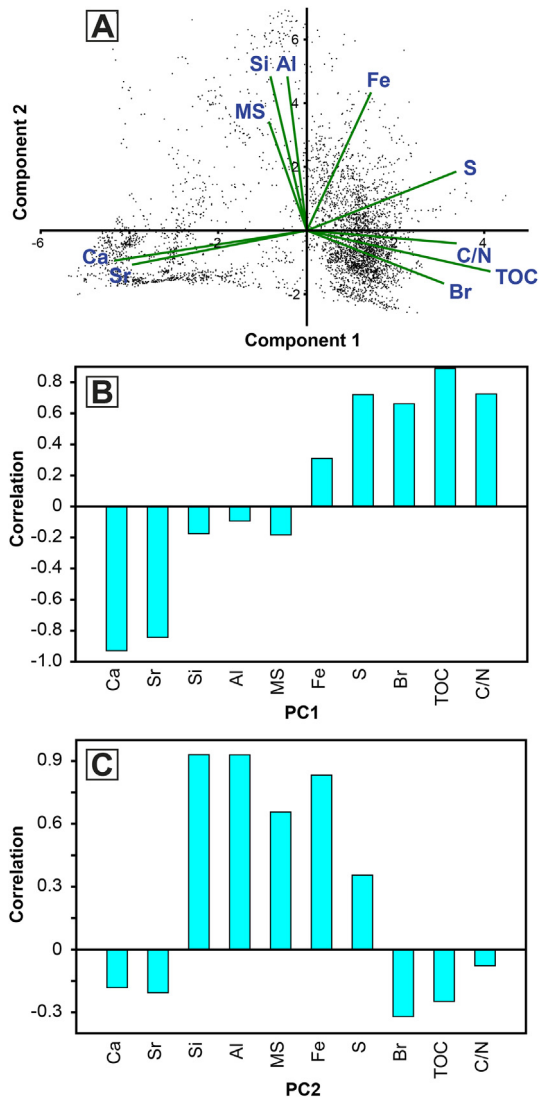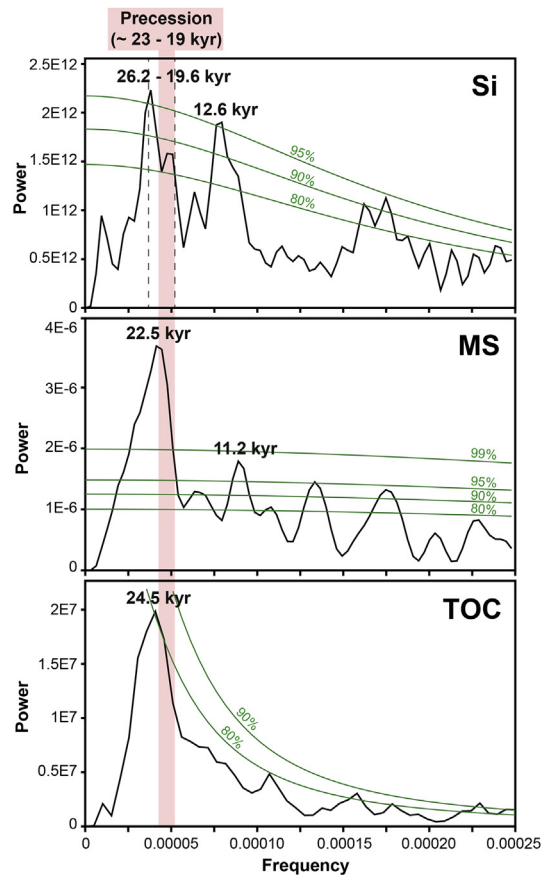
Fig. 7. The Principal Component Analysis (PCA) from Ca, Sr, Si, Al, Fe, S, Br, MS, TOC and C/N data from Padul-15-05 showing: (A) the scatter plot with PC1 and PC2 axis variations, and (B) PC1 and (C) PC2 variations on loading plots.


Fig. 8. Spectral analysis results performed on Si, MS and TOC data from Padul-15-05. Main periodicities as well as confidence intervals (green line) are shown. Dashed lines mark the age range of a same period. The age range of the precession cycle (~23–19 kyr) has also been marked. (For interpretation of the references to color in this figure legend, the reader is referred to the Web version of this article.)

averages 11% for these samples. More important is the uncertainty derived from extrapolating ages beyond the calibration data (beyond 14 kyr), which is significant for this core (Fig. 3). The age model is highly sensitive to the choice of mathematical function used to infer the rate of racemization beyond the calibration. A rough estimate of the age uncertainty is at least ±20%.

Given the above assumptions, the AAR data can be used to estimate the age of four undated samples (at 13.13 m, 22.98 m, 23.37 m and 23.42 m depth) (Fig. 3 and Table 3). The three AAR ages on gastropods from 23.42 to 22.98 m depth range from 107 to 133 kyr, but are in reversed stratigraphic order. We consider the three ages to be within errors of one another and take the mean age (118 kyr) to represent the mean sample depth (23.26 m).

4.1.3. Sediment accumulation rates (SAR)

The age-depth model from 23.27 m to 42.64 m depth was made using linear extrapolation with calculated sedimentation rates from the radiocarbon-dated part of the Padul-15-05 core because of the lack of age control points below 23.27 m. The sedimentation rate of the peat lithology (SARpeat) was calculated according to the well

dated Holocene interval (from 1.23 m to 3.65 m depth) while the carbonate/marl SAR (SARcarb) was calculated based on the well dated carbonate/marl intervals from the last glacial period and deglaciation (from 3.85 m to 5.82 m depth). Therefore, the obtained peat SAR was 0.365 mm/yr whereas carbonate/marl SAR was 0.152 mm/yr (Fig. 2). SARcarb was used from 23.27 m to 28.78 m depth in accordance with the carbonate-rich sediments that dominate this interval. Age control through three small carbonate/marl intervals at 39.26–39.53 m, 40.10–40.82 m and 41.39–41.72 m depth was extrapolated using SARcarb as well. SARpeat was used from 28.78 m down to the bottom (42.64 m), in accordance with the peat-rich sediments that dominate this interval. Following this method, the base of the Padul-15-05 core would have an age of ~197 kyr BP (Fig. 2).

4.2. Principal component analyses (PCA)

The Principal Component 1 (PC1) obtained from the PCA accounts for 40.1% of the total variance with positive correlation between S, Br, TOC and C/N, and negative correlation to Ca and Sr. The Component 2 (PC2) accounts for 32.3% of the total variance and is mainly controlled by Si, Al, Fe and MS. The rest of the Principal Components were not included because they represent low percentages of the total variance (<9%). Scatter and loading plots are represented in Fig. 7 while PC1 and PC2 scores for the entire core are given in Fig. 9.
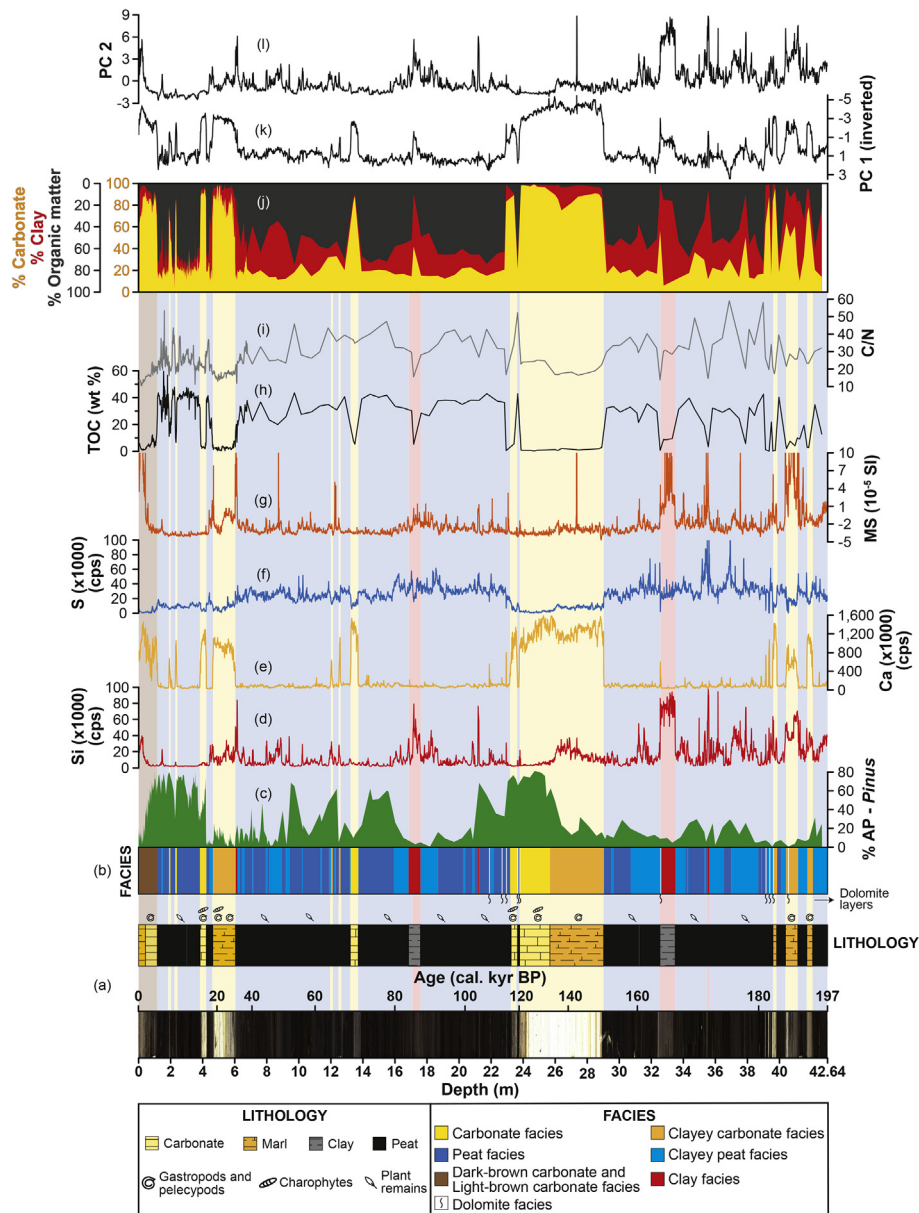
Fig. 9. Multiproxy data comparison with respect to depth from the Padul-15-05 sedimentary record. From bottom to top: (a) scanner photography with the correspondent lithology and organisms (gastropods, pelecypods, charophytes and plant remains); (b) facies also showing the occurrence of thin dolomite facies/layers; (c) Arboreal Pollen percentages (AP) with *Pinus* excluded from the total terrestrial pollen sum; (d) Si data in cps; (e) Ca data in cps; (f) S data in cps; (g) magnetic susceptibility in SI; (h) TOC in weight percent; (i) C/N; (j) carbonate, clay and organic matter percentages; (k) PC1 values (inverted) and (l) PC2 values.

4.3. Lithology and sedimentary facies

The lithology of the Padul-15-05 core begins with peat sediment at the bottom (42.64 m depth) until 28.78 m depth, with 3 thin marl layers at 41.71−41.38 m, 40.81−40.24 m and 39.52−39.33 m depth and a thin clay layer at 33.22−32.35 m depth. From 28.78 m to 25.44 m depth marls are predominant, transitioning to carbonate sediments until 23.57 m depth. From 23.57 m to 5.98 m depth lithology is mainly composed of peat, but a clay layer is present at 17.43−17 m depth and a carbonate layer is present at 13.58−13.13 m depth. Marls occur again between 5.98 m and 4.57 m depth, followed by a thin peat layer from 4.57 m to 4.19 m depth, which is then followed by a thin carbonate layer at 4.19 m−3.82 m depth. Peat sediments are again deposited from 3.82 m to 1.15 m depth. The topmost 1.15 m of the core is characterized by brown carbonates and marls (Fig. 9).

Lithological features as well as the most representative inorganic geochemistry data (Ca, Si, S), magnetic susceptibility, TOC (wt %), C/N, color lightness and the PCA results were used for the facies classification of the core (Table 5). According to their presence in the core, we distinguished four main facies (*Peat facies*, *Clayey peat facies*, *Clayey carbonate facies* and *Carbonate facies*) and four secondary facies (*Dark-brown carbonate facies*, *Light-brown carbonate facies*, *Clay facies* and *Dolomite facies*). Every secondary facies represents less than the 5% of the total depth of the core. Note that Ca shows very similar trends compared to Sr, lightness and b* values, while Si covaries with Fe, Al, K, Zr, Rb/Sr and MS. Finally, S shows a good correlation with Br, TOC and C/N (Figs. 4 and 9). Correlation coefficients of the different proxies are also shown in Table 4. Data from different facies described below are presented in Fig. 9 and in Table 5.

4.3.1. Clayey carbonate facies

Yellowish carbonates with internal cm-to dm-clayey layers, occur between ~42 and 39 m (~194–182 kyr BP), at ~ 29–25.5 m (~154–133 kyr BP) and at ~ 6–4.6 m depth (~29–18 kyr BP). Charophytes, gastropods and pelecypods are very frequent, while plant remains are not common. Mineralogy is composed of calcite, dolomite and quartz. Inorganic geochemistry yields high relative values in Ca (>800,000 cps), medium values in Si (15,000–30,000 cps) and low values in S (5000–25,000 cps). Magnetic susceptibility (<1 × 10^{-5} SI), C/N (20–30) and TOC (0–3%) is low. Lightness is high (70–100%). PC1 is characterized by low values and PC2 by medium values.

4.3.2. Carbonate facies

This facies is characterized by light yellowish carbonate mainly composed of calcified remains of charophytes, and occurs at ~25.5–23 m (~133–117 kyr BP), 13.58–13.13 m (~71–69 kyr BP) and at 4.19–3.82 m depth (15.5–12.6 kyr BP). There are also high occurrences of gastropods and pelecypods, while plant remains are rare. Calcite is the principal mineral. According to inorganic geochemistry, Ca shows high relative values (>800,000 cps) while Si (0–10,000 cps) and S values (0–6000 cps) are low. Magnetic susceptibility (<-2 x 10^{-5} SI), TOC (0–3%) and C/N (15–25) are also low, while lightness is high (70–100%). Values for PC1 and PC2 are low.

4.3.3. Peat facies

Black massive peat with high amounts of organic matter and plant remains occurs in different sections throughout the core. There are no gastropods, pelecypods or charophytes in this facies. Mineralogical analysis shows very flat diffractograms, with very occasional rare quartz. According to inorganic geochemistry, this facies characterized by high relative S values (10,000–75,000 cps), and low Ca (20,000–100,000 cps) and Si (0–4000 cps) values. Magnetic susceptibility (<-3 x 10^{-5} SI) and lightness (25–40%) are also low. Both TOC (30–60%) and C/N (35–60) values are high. PCA analysis yields positive PC1 and negative PC2 values.

4.3.4. Clayey peat facies

Clayey organic peat with some plant roots is normally intercalated with the *Peat facies*. As in the *Peat facies*, there are no gastropods, pelecypods or charophytes. Quartz and illite are the main minerals in the diffractograms. Inorganic geochemistry shows high relative Si (10,000–85,000 cps) and S values (10,000–75,000 cps) and low Ca (20,000–100,000 cps) values. Magnetic susceptibility has medium relative values (<3 × 10^{-5} SI), whereas TOC (20–40%) and C/N (25–40) are high. Lightness (25–50%) is low. This facies is characterized by positive PC1 and relatively high PC2 values. The *Clayey peat facies* and the previous *Peat facies* make up approximately a 73% of the total facies in the core. The intercalation between these two facies is common.

4.3.5. Dark-brown carbonate and Light-brown carbonate facies

These two secondary facies are characterized by light to dark carbonates that occur in the topmost part of the core (1.15–0 m, 4.7–0 kyr BP). Inorganic geochemistry for both facies yield high relative Ca values (>200,000 cps), medium Si (0–40,000 cps) values and low S (0–8000 cps) values. Magnetic susceptibility varies from low to high (from −4× 10^{-5} to 30 × 10^{-5} SI). Both TOC (0–10%) and C/N (0–25) values are low, while color lightness is high (40–80%). Specifically, the *Dark-brown carbonate facies* (1.15–0.4 m depth) is principally composed of calcite without detrital sediments (no dolomite, quartz, illite, and low values of Si and MS). Charophytes, gastropods and pelecypods are more abundant than in the *Light-brown carbonate facies* (0.4–0 m depth). PCA yields low values for PC1 and PC2. On the contrary, the *Light-brown carbonate facies* presented calcite, dolomite, quartz and illite. Silicon, MS and PC2 values in this facies are higher, while PC1 is also low.

4.3.6. Clay facies

This secondary facies consists of brown organic clayey layers with occasional mottling and mixed sediment textures that occur at ~33.2–32.3 m (~166–164 kyr BP) and ~17.4–17 m depth (~87–81 kyr BP). Other thin layers (<10 cm thick) appear at ~ 35.3 m (~172 kyr BP), ~21 m (~104 kyr BP) and ~6 m depth (~29 kyr BP). There is occasional presence of plant roots. Mineralogy is mainly composed of quartz and illite. Inorganic geochemistry yields high relative values of Si (20,000–95,000 cps), medium values of S (20,000–45,000 cps) and low values in Ca (30,000–100,000 cps). Magnetic susceptibility varies from low to high (from −2× 10^{-5} to 15 × 10^{-5} SI). Both TOC (0–10%) and C/N (15–30) are low, while lightness is medium (45–60%). PCA yields relatively low PC1 but high PC2 values.

4.3.7. Dolomite facies

This secondary facies is formed by ten grayish-whitish dolomitic sediment layers (maximum thickness of 7 cm) randomly distributed in the lower half of the core between 40.2 and 38.8 m (~187–181 kyr BP), at 32.3 m (~164 kyr BP) and between 23.5 and 21.7 m depth (~120–108 kyr BP). Mineralogy is mainly dolomitic, with occasional quartz. Inorganic geochemistry yields high relative Ca (>700,000 cps), high Si (20,000–60,000 cps) and low S (0–5000 cps) values. Magnetic susceptibility (<-1 x 10^{-5} SI), TOC (0–1%) and C/N (20–25) values are all low. This facies is characterized by the absence of plant remains, charophytes, gastropods and pelecypods. Lightness is high (95–100%). PCA is characterized by low PC1 and PC2 values.

4.4. Pollen results

The Arboreal Pollen (AP) percentage (excluding *Pinus*), shows important abundance variations throughout the Padul-15-05 core. Values are relatively low (average value of ~17%) at the bottom of the core between 42.64 m and ~26 m depth (~196–135 kyr BP). At ~26 m depth (~135 kyr BP) AP begin to develop, reaching its maxima at ~24.5 m depth (~126 kyr BP) with ~82% of the pollen assemblage. A decrease in AP values occur between ~22.5–22 m depth (~115–111 kyr BP) before another increase until ~21 m depth (~105 kyr BP). Between ~21 m and ~16 m depth (~105–80 kyr BP), average AP values are around 13%, with highest peaks never exceeding a 27%. Thereafter, relatively high percentages occur (maxima of ~60%) between ~16 m and ~13.5 m depth (~80–73 kyr BP), as well as between ~12–9.5 m depth (~65–53 kyr BP), with maximum values at ~65 kyr (maxima of ~62%) and ~53 kyr BP (maxima of ~69%). During the last glacial period (~9.5–4.19 m depth, ~53–15.5 kyr BP), AP percentages decline to average values of ~12%. Finally, from 4.19 m to the core top (from 15.5 kyr to the present), AP increases with an average value of ~50% and a maximum peak of ~81% (Figs. 9 and 10).

4.5. Spectral analysis

Statistically significant spectral cyclicities at ~26.2 kyr (>95% CI) and ~19.6 kyr (>80% CI) are present in Si, which are probably pointing into the same cycle. A ~24.5 kyr cycle (>80% CI) is present in the TOC while in MS occur at ~22.5 kyr (>99% CI). A cycle of ~12.6 kyr (>95% CI) in Si and ~11.2 kyr (>95% CI) in MS are most likely the harmonics of the ~26.2–19.6 kyr and 22.5 kyr cycles, respectively. We focused on the highest amplitude cycles so smaller scale periodicities have not been described. Note that the spectral analysis on

Si was developed using Si data in counts per second (cps) due to its better results and representation with respect to normalized Si. However, both Si data time-series present very similar trends with a correlation coefficient of 0.807.

5. Discussion

### 5.1. New age control for the Padul sedimentary sequence

This study has improved the age control of the Padul sedimentary sequence compared with previous works through a large number of AMS radiocarbon ages (a total of 61 samples analyzed), specific-compound radiocarbon dating and amino acid racemization (AAR) in gastropods from the Padul wetland. The lack of tephras in this part of the western Mediterranean region (Satow, 2012), the lack of siliciclastic-rich sands/clays that could be used for optically stimulated luminescence (OSL), and issues related to U/Th ages in an open wetland system that preclude obtaining accurate U/Th dates (Sierralta et al., 2017), led us to the AAR dating method for dating sediment older than the radiocarbon limit. In absence of independent numerical ages for the bottom part of the core, we decided to use the sediment accumulation rates (SAR) of the two main lithologies (peat and carbonate/marl) from the well-dated top part of the core, with the purpose of creating a relatively objective age-depth model for the entire Padul-15-05 core. Tuning was avoided in order to elude circular reasoning (Blaauw, 2012). A spectral analysis in the depth domain of the silicon data and a

subsequent filtering based on the obtained frequency ($f = 0.0018762$) was also developed to identify the periodicity of the lithological changes and to compare with insolation cycles. This cyclostratigraphic exercise supports the age model for the Padul-15-05 record, agreeing with the total number of cycles that occurred in the last ~197 kyr obtained in the age-depth model and related with insolation (Supplementary Fig. S1).

5.2. Facies, environment, climate and lake level reconstruction

Depositional environments and lake level reconstruction at Padul were determined based on the different previously described proxies and facies. Sedimentary facies changed through time due to paleoenvironmental changes depending on climate changes and lake level response (Figs. 10 and 11; Table 5). Lake level of the Padul-15-05 core was reconstructed using the smoothed PC1 score that included the most representative multiproxy data (Ca, Sr, Si, Al, Fe, S, Br, TOC, C/N and MS). Negative PC1 scores with positive correlation between Ca and Sr and opposite to S, Br, TOC and C/N (Figs. 7 and 9) suggest high lake level related to carbonate/marl precipitation (*Clayey carbonate facies* and *Carbonate facies*). In contrast, positive PC1 scores could be indicative of low lake level during peat formation (*Peat facies* and *Clayey peat facies*) with high amount of organic matter and abundant littoral emerged vegetation. Below we give a more extended interpretation of the different identified facies in terms of environmental conditions:

Clayey carbonate facies is interpreted here as being deposited
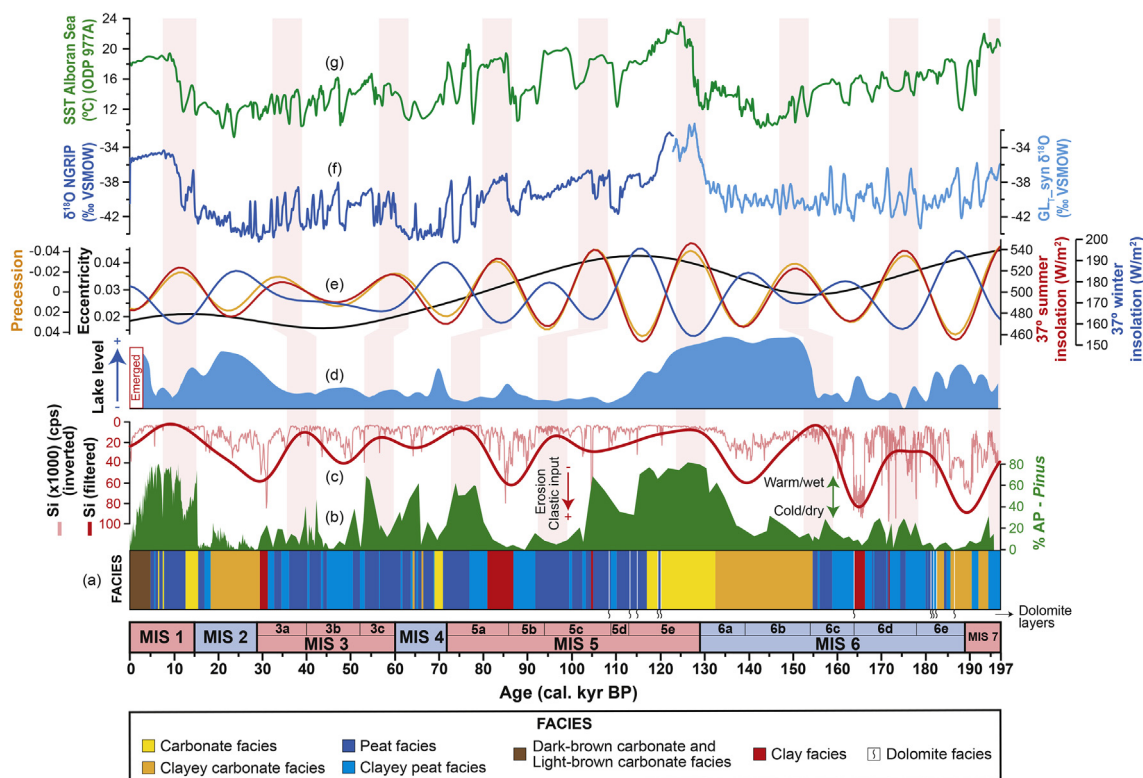
Fig. 10. Representation and interpretation of different proxies from Padul-15-05 with respect to age showing: (a) facies with the presence of thin dolomite layers; (b) Arboreal Pollen (AP) percentages with *Pinus* excluded from the terrestrial pollen sum, indicating warm/wet or cold/dry climate; (c) Si values in cps (light red) (inverted) and filtered Si data (red) indicative of erosion and clastic input and/or biogenic dilution; (d) lake level reconstruction based on smoothed PC1 data; (e) summer insolation at 37°N (red), precession (orange) and eccentricity (black); (f) δ¹⁸O values from NGRIP and GL_syn δ¹⁸O records (‰ VSMOW) and (g) Sea Surface Temperature (SST) record from Alboran Sea (°C). Light red vertical bands show correlation between minima in Si and maxima in summer insolation. Marine Isotope Stage (MIS) 6 and substages have been ascribed following Table 1 from Sun and An (2005). MIS 5 and substages are based on the SST from Martrat et al. (2004) and vegetation data from Milner et al. (2016). Finally, MIS 4, 3, 2 and 1 have been delimited according to vegetation changes from Fletcher et al. (2010). (For interpretation of the references to color in this figure legend, the reader is referred to the Web version of this article.)

during highest lake level stages with frequent occurrences of gastropods and pelecypods. Detrital input characteristic from this facies occurred during increasing regional aridity, resulting in less forest cover/barrier in the nearby Sierra Nevada and the Padul area (see low AP in Fig. 10) and intensifying the erosion during the coldest and most arid climate conditions. As also occurred in Lake Ohrid explained by Francke et al. (2016), enhanced physical weathering and erosion could be due to an intensification of glacial and/or periglacial activity. The PC2 in the PCA shows positive correlation of Si, Al, Fe and MS, also pointing towards predominant detrital deposition, likely linked to higher clastic input from Sierra Nevada (Figs. 7, 9 and 11A) and/or minor biogenic productivity in the lake. This *Clayey carbonate facies* mainly occurred during minima in summer insolation and low eccentricity during MIS 6b and 6a (~29—25.5 m) and again during MIS 2 (~6—4.6 m) (see Figs. 9 and 10), indicating that this is the coldest-related facies in the core. The three clayey carbonate facies bands between ~195 and 182 kyr BP also largely correspond to a period of minimum insolation, suggesting cold and arid phases, even if eccentricity was not at the lowest values. Vaks et al. (2003) and Hodge et al. (2008) show that during glacial periods, Mean Temperature of the Warmest Month (MTWA) and Mean Annual Temperature (TANN) in the Mediterranean region reduced while Effective Annual Precipitation (EAP) (precipitation/evapotranspiration balance) increased. Therefore, strong cold conditions and absence of evapotranspiration would result in high lake level at Padul (Fig. 11A). The occurrence of glaciers at higher elevations in Sierra Nevada during glacial periods could also be an important source of water to lower elevation areas, through increased aquifer discharge during slightly warmer summers, and therefore, could also contribute to a high water table at Padul.

Carbonate facies is also interpreted here as indicative of relatively high lake level, which would enable the proliferation of organisms, such as charophytes, gastropods and pelecypods, organisms that would increase carbonate sedimentation. The maximum lake level should not have been excessively high, because charophytes typically grow in water depths of only a few meters (<4 m) (Cohen, 2003; Pelechaty et al., 2013). Even if the water contained abundant dissolved carbonate and was supersaturated in these elements, a triggering mechanism is needed in order to precipitate carbonate, such as an increase in CO_2 degassing (Jones and Renaut, 2010) or the activity of calcifying charophytes (Pentecost, 2005). Negative PC1 values, with a strong correlation between Ca and Sr (opposite to S, Br, TOC and C/N), are characteristic of this facies (Figs. 7 and 9). The absence of detrital input from Sierra Nevada also indicate less weathering and erosion, perhaps pointing to warmer conditions and/or probably higher biogenic deposition. Several previous works (Ortiz et al., 2004a; Magny et al., 2007) also interpreted this facies as deposited in relatively deep lake waters. This facies typically started right after minima in insolation, and thus, during warming transitions, such as Termination II after the penultimate glacial period or Termination I after the last glacial period (Figs. 10 and 11B). A high water table in Padul at these times would be closely related to the melting of snow/ice that accumulated in Sierra Nevada during the preceding cold phases (as explained above in *Clayey carbonate facies*), suggesting a delay in the response of the lake system during increasing summer insolation after glaciations. Thereafter, lake level remained relatively high for a period of time (~3000 years for the last deglaciation; ~15.5—12.6 kyr BP) until glaciers disappeared, aquifer discharge diminished, and lake level decreased due to evapotranspiration. However, *Carbonate facies* should have not only be related to water input from glacier melting, but also rainwater supply during high moisture climate conditions greatly exceeding evapotranspiration in the lake resulting in positive EAP, as occurred during the MIS 5e (see Section 5.3.2). A similar carbonate layer occurred between 13.13 and 13.58 m depth (~71—69 kyr BP; early MIS 4), but this interval has a different color, with lower lightness, yields much lower AP values (<12%), slightly higher TOC percentages and higher C/N ratio (Figs. 4 and 9), not representing either a
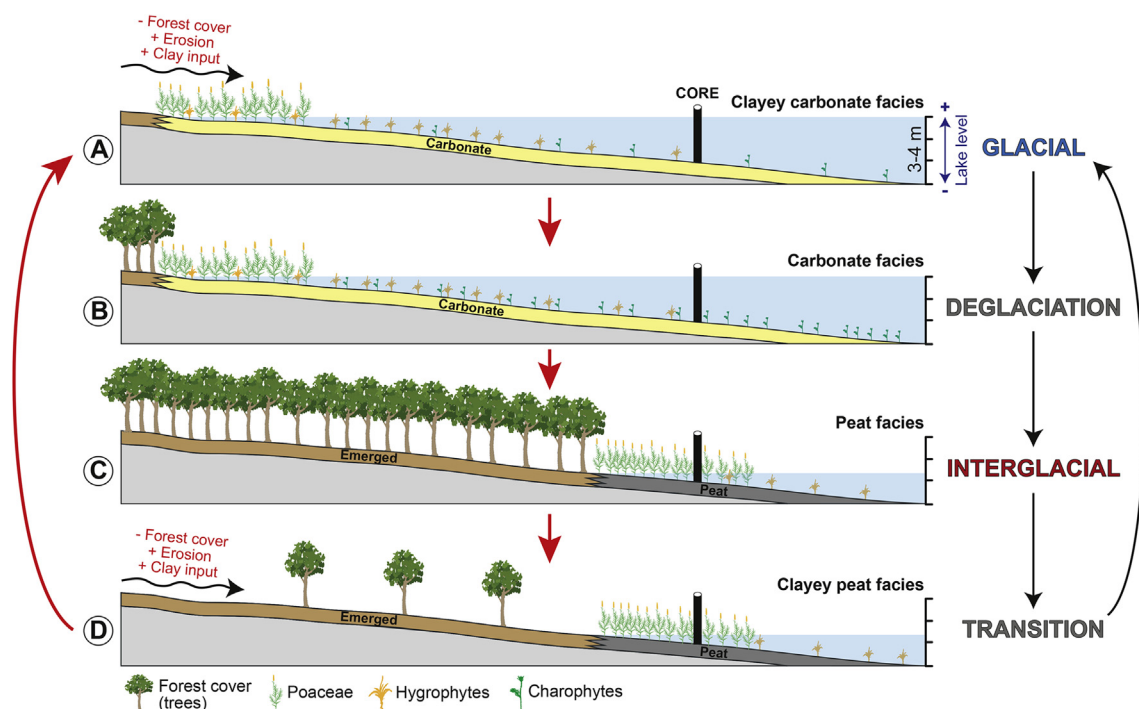

Fig. 11. Schematic representation of different glacial, deglaciation, interglacial and transition phases with respect to *Clayey carbonate*, *Carbonate*, *Peat* and *Clayey peat* facies, respectively, from Padul-15-05 record. Each climatic period shows different sedimentation, lake level and vegetation.

deglaciation nor an interglacial period. High C/N ratio would indicate low presence of nitrogen from algae and aquatic plants (Meyers, 1994), so the lake level was also probably lower. A similar facies layer occurred in the Holocene part of the core at 7.5 kyr BP, which might signify shallow lake environments but under cold and arid climate conditions (Ramos-Román, 2018).

Peat facies can be interpreted as deposited in very shallow palustrine environments with littoral vegetation and large accumulation of organic matter promoting anoxic conditions in the sediment during degradation. This is confirmed by the PCA, showing a positive PC1 with very good correlations between S, Br, TOC and C/N (Figs. 7 and 9). This correlation between Br and TOC has also been observed in a sedimentary records from the Gulf of Cadiz in the southwest Iberian Peninsula (Bahr et al., 2014). C/N ratios greater than 20 are characteristic of cellulose-rich vascular land plants, while mixture of vascular and algal plants shows values between 12 and 17 (Ertel and Hedges, 1985; Meyers, 1994). High C/N values in this facies indicate that the organic matter originated from vascular plants. Pollen data, along with the absence of siliciclastics in this facies show that the forest cover was relatively high around Padul and Sierra Nevada, and consequently, the weathering/erosion in the catchment basin was low and/or the biogenic productivity in the lake probably higher. Therefore, *Peat facies* is interpreted here as developed during high summer insolation under relatively warm and regionally humid periods as shown by the Arboreal Pollen data (e.g., MIS 5a and Holocene) (Fig. 10), and similar to that recorded in Lake Accesa during the Holocene by Magny et al. (2007). High summer insolation would have triggered enhanced land-sea temperature contrast, producing more cyclonic activity and fall-winter precipitation in the area. Climate during peat formation was then characterized by strong seasonality with maximum summer drought and high winter precipitation, but evapotranspiration mainly during summer due to maxima in summer insolation greatly exceeded aqueous input (low effective precipitation), resulting in very low lake level (Figs. 10 and 11C). This would agree with several previous works, such as Ortiz et al. (2004a) at Padul, Magny et al. (2007) at Lake Accesa or García-Prieto (2015) at El Cañizar Lake, who also interpreted peat sedimentation as being produced during episodes of low water depth. Shallow wetland environments would favor abundant emerged vegetation that could trigger anoxia during periods of high productivity and high water temperature (Cohen, 2003).

Clayey peat facies results from the combination of peat formation and detrital input. This facies is interpreted as deposited during low lake level, but when water levels were slightly higher than during the sedimentation of *Peat facies*. Therefore, this facies is transitional between peat (interglacial/interstadial) and clayey carbonate (fully glacial) facies. *Clayey peat facies* is interpreted as typically occurring during the transition between insolation maxima and minima, and during arid and cool stadials. The detrital component (shown by positive PC2 values with good correlations between Si, Al, Fe and MS), generally interpreted as fluviatile sediments carried into Padul from Sierra Nevada and/or lower biogenic productivity, could be due to enhanced erosion during these climate conditions. Relatively low summer insolation might produce colder and/or drier conditions that would have prevented the expansion of forest cover/barrier, and therefore, would have resulted in increased siliciclastic input to the lake from Sierra Nevada, as occurred for example during the MIS 3 (in particular between ~30 and 50 kyr BP) (Figs. 10 and 11D). High rates of sediment transport linked to open landscape vegetation can be observed in the alluvial fan systems from Lahontan and Mojave (USA; Harvey et al., 1999) and in the lacustrine record of El Cañizar Lake (Spain; García-Prieto, 2015).

Clay facies is characterized by important detrital content (Si, Al, Fe, K, Zr, Ti, Rb/Sr, MS and positive PC2 values of the PCA) (Figs. 4, 7 and 9). Similar to *Clayey peat facies* explained above, it occurred during insolation minima and thus could be interpreted as occurring during cold-arid abrupt stages, when erosion increased because of the low forest cover, such as during MIS 5b (~5000 years delay probably due to dating uncertainties) (Fig. 10). This facies shows that lake level should not have been very high due the presence of mottling textures that are associated with ephemeral lake margin environments and that are indicative of oxidizing-reducing conditions (Buurman, 1980; Wells, 1983; Alonso-Zarza et al., 1992).

Dolomite facies is defined by several centimeters-thick dolomite laminae with some quartz (Fig. 6; Table 5), which could be related to episodes of high runoff or fast tectonic pulses resulting in dolomite sedimentation carried from the Triassic dolomitic complex from Sierra Nevada. However, we cannot ruled out dolomite precipitation due to cyanobacterial degradation during evaporation/desiccation stages as recorded in shallow ephemeral lakes from Coorong region in Australia (Wright, 1999), or the authigenic precipitation linked to sulfate reducing bacteria under anoxic conditions as occur in modern hypersaline lakes from Spain (Corzo et al., 2005).

Dark-brown carbonate facies and *Light-brown carbonate facies* occur in the topmost part of the core (the last ~ 4.5 kyr BP) and could be interpreted as deposited in a shallow and a seasonal lake environment, respectively (Fig. 9; Table 5). *Dark-brown carbonate facies* (~4.5–1.5 kyr BP) probably corresponded to shallow lake phases, allowing the presence of carbonate-shell organisms such as gastropods, pelecypods and charophytes to produce carbonate sediments. *Light-brown carbonate facies* (the last ~ 1.5 kyr) would correspond to ephemeral/dried lake stages preventing both very shallow palustrine sedimentation (peat formation) and deeper lake signals (carbonate with gastropods, pelecypods or charophytes). For a more detailed interpretation of lithology and facies of the last ~4700 years from the Padul-15-05 core, see Ramos-Román et al. (2018a).

5.3. An idealized orbital cyclic pattern in Padul (from MIS 6 to MIS 1): integrating orbital variability, vegetation, facies and lake level

Glacial/interglacial oscillations had an influence on lake levels at Padul, and thus, on the sedimentation (i.e., facies). This is deduced by the studied proxies at Padul, which show similar patterns with respect to paleoclimate variations (i.e., insolation), allowing us to reconstruct an idealized climate-vegetation-lake level-sedimentation cyclic pattern, based on and modified from previously published climate-vegetation cycles from Turner and West (1968), Combourieu-Nebout (1993), Bertini (2001) and Tzedakis (2007) (Fig. 12). The idealized cyclic patterns represented in Fig. 12 summarize different facies deposition along with their respective lake level, climate and specific vegetation (Camuera et al. in prep.) for the last glacial-Holocene interglacial cycle and for the penultimate glacial-last interglacial cycle. Both idealized cyclic patterns start from Phase 1 (*Clayey carbonate facies*; number 1 in Fig. 12) during the glacial period, passing through the Phase/number 2 (*Carbonate facies*) during deglaciations and in the case of the last interglacial cycle also during the interglacial maxima. Phase/number 3 (*Peat facies*) occurred during the Holocene interglacial maxima and mainly during interstadials in both cycles. The alternation between Phases/numbers 3 and 4 (*Peat facies* and *Clayey peat facies*) suggest fluctuations in insolation during interglacial-glacial transitions, representing maxima and minima in insolation, respectively.

Spectral analyses on different proxy time series (Si, MS and TOC) show statistically significant periodicities between ~26.2–19.6 kyr, which are concordant with the orbital precession cycle (~23–19

kyr) (Milankovitch, 1920; Imbrie and Imbrie, 1980; Berger et al., 1998) (Fig. 8). Silicon was filtered based on the average frequency from the 26.2 kyr and 19.6 kyr cycles (4.4497E-05) using the Analyseries 2.0 software (Paillard et al., 1996) and compared with insolation (Fig. 10). This data are most likely indicating that siliciclastic deposition in the lake was enhanced during minima in summer insolation due to intensified weathering and/or erosion, favored by less forest cover in Sierra Nevada and around Padul during cold and arid climate conditions (Fig. 11A and D). This is supported in Padul by the pollen analysis, where the lowest arboreal pollen values coincide with Si maxima and insolation minima (Fig. 10), as also indicate the negative correlation coefficient of −0.53 ($p = 3.5763E-31$) between Si and the Arboreal Pollen data.

High-resolution multiproxy analyses in the Padul-15-05 record show strong similarities with Marine Isotope Stages (MISs), as well as with Alboran Sea Surface Temperature (Martrat et al., 2004), $GL_T\_syn\ \delta^{18}O$ synthetic isotope record (from the base of the Padul core −197 kyr-to 123 kyr) (Barker et al., 2011) and $\delta^{18}O$ record from North Greenland (from 123 kyr to the present) (NGRIP-Members, 2004) at orbital glacial/interglacial and sub-orbital stadial/interstadial time scales (Fig. 10). Below is a description of the main paleoenvironmental (lake level and facies) and paleoclimate oscillations observed in Padul-15-05 record with respect to global climate oscillations (i.e., MIS oscillations).

5.3.1. Glacial and cold stadial periods

The coldest and driest glacial conditions in the Padul-15-05 record are characterized by *Clayey carbonate facies*, occurring during MIS 6b and 6a at ~155–132 kyr (~29–25.5 m depth) and during MIS 2 at ~29–18 kyr BP (~6–4.6 m depth) (Figs. 9 and 10). High lake levels occurring at those times in Padul, were most likely due to low evaporation, and thus, high Effective Annual Precipitation (EAP). This seems to agree with General Circulation Models from Kutzbach and Guetter (1986) and COHMAP Members (1988) and corroborated by the study of Harrison and Digerfeldt's (1993) about lake level responses during glacial periods. They suggest that colder Sea Surface Temperature (SST) and the development of a fixed anticyclone over the North European ice sheets during glaciations generated a cold/dry storm track from the western Atlantic into the

Mediterranean region that produced cloudy summers (with no precipitation) and also brought cold/dry air masses from the North European glacial anticyclone into the Padul area during winter times. Besides, Prentice et al. (1992) also suggested cool and dry summer climate for the Last Glacial Maximum (LGM) (which could be extrapolated to other glacial periods), even if winter precipitation models were not completely clear. Therefore, cold conditions during both seasons and a reduction in evaporation rates during cloudy summer times resulted in positive precipitation-evapotranspiration balance and high EAP (even with low winter precipitation), and high lake level. Moreno et al. (2012) in Villarquemado paleolake (central Spain) also suggested high lake level conditions for carbonate lake environments as a consequence of cold and relatively humid climate during the LGM, while Vegas et al. (2009) in Fuentillejo maar (central Spain) showed low lake levels during arid climates. It should also be noted that even if glaciers at high elevations of Sierra Nevada were not the main water sources at Padul, they could have also provided some water supply to lower areas (i.e., Padul lake) due to partial melting during slightly warmer summer times.

The lower Si content during the early MIS 6b (~155–144 kyr BP) with an slight increase in AP at ~ 145 kyr compared to the late MIS 6b and early MIS 6a (~144–137 kyr BP), could be related to a more temperate and humid climate, resulting from higher summer insolation but still under lowest eccentricity, as shown in the Ioannina pollen record from Northern Greece at 150 kyr (Tzedakis et al., 2003a). In addition, a slight more humid climate under overall cold climate conditions could have allowed higher EAP than previously in the Sierra Nevada area, and therefore, the beginning of high lake level clayey carbonate formation during MIS 6b at around 155 kyr ago. The coldest and most arid conditions of the last part of the penultimate glacial period occurred between ~145 and 137 kyr (~27.3–26.2 m depth), with *Clayey carbonate facies* with high siliciclastic input due to low lacustrine productivity and/or high weathering/erosion favored by low forest cover during minimum summer insolation just after minimum eccentricity (Figs. 10 and 11A), agreeing with coldest conditions recorded in by SST in Alboran Sea (Martrat et al., 2004).

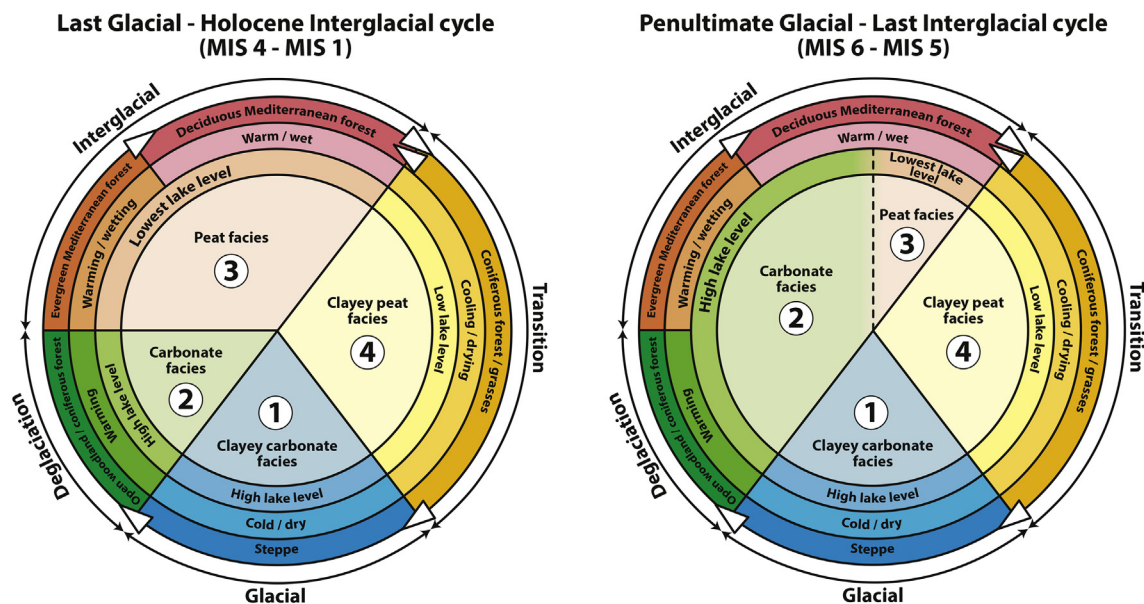*Clayey peat facies* characterized by relatively low AP and high Si

Fig. 12. Idealized Facies-Lake level-Climate-Vegetation patterns for the Last Glacial-Holocene Interglacial cycle (left) and Penultimate Glacial-Last Interglacial cycle (right). White arrows in the external part show the direction of the change.

content also interpreted as relatively cold and arid regional conditions occurred mainly during MIS 6d, 6c, 5b, 5a, 3b and 3a. The low forest cover indicated by the low AP percentages and subsequent high siliciclastic input in the lake fit well with minima in summer insolation. High Si values in Padul during MIS 6e through 6c at ~190–155 kyr BP (~42–29 m depth) suggest cold/arid climate and *Clayey peat facies* deposition with low EAP between ~ 180 and 155 kyr, agree well with stable isotope-based paleoclimatic records from Gitana Cave ($\delta^{13}C$) in the southern Iberian Peninsula (Hodge et al., 2008) and from Soreq Cave ($\delta^{13}C$, $\delta^{18}O$) in the eastern Mediterranean (Bar-Matthews et al., 2003). With respect to the MIS 5b stadial, is characterized by low summer insolation with low AP development and high siliciclastic input (*Clay facies* and *Clayey peat facies*), suggesting cooler and drier climate. This would be a result of low summer and high winter insolation that could lead to lower summer evaporation, and therefore, lower winter precipitation, similar to that explained by Berger et al. (2007) for the Post-temperate transition at 115 kyr BP. Nevertheless, it should be mentioned that maximum Si data and *Clay facies* at ~87–81 kyr BP present a delay with respect to minimum summer insolation at ~92 kyr BP, probably due to lack of age control samples at this depth. Finally, note that the alternation between *Clayey peat facies* and *Peat facies* was very frequent throughout the Padul-15-05 core probably due to smaller millennial climate oscillations (i.e., D-O and Heinrich-like variability).

5.3.2. Interglacial and warm interstadial periods

Interglacial and interstadial periods in the Padul-15-05 record are mainly characterized *Peat facies* with lack of siliciclastic input and high AP percentages (Figs. 9 and 10). The early and middle Holocene (12.6–4.5 kyr BP) as well as interstadials are characterized by this lithology, suggesting climate warming that enhanced evapotranspiration in the lake, exceeding rain/groundwater input and decreasing the EAP and lake level. This is in agreement with other Mediterranean records such as Lake Accesa in north-central Italy, which also shows peat lithology during the early and middle Holocene (Magny et al., 2007). In addition, low lake levels during maximum summer insolation have also been described in different records from the Iberian Peninsula, such as in Villarquemado paleolake (Aranbarri et al., 2014), Lake Estanya (González-Sampériz et al., 2017) and Lake Banyoles (Valero-Garcés et al., 1998), and summarized in Morellón et al. (2018). Nevertheless, almost the entire MIS 5e (~132–117 kyr BP) in Padul is characterized by *Carbonate facies*, suggesting different environmental conditions during the last interglacial in the Padul area. *Carbonate facies* could have been related to prolonged glacier melt-water supply to this area, as occurred during the deglaciation after the last glacial period (15.5–12.6 kyr BP). However, sedimentation of the ~15,000 year-long carbonate deposits during the MIS 5e could have also been related to a wetter climate. Temperature reconstructions by Kaspar et al. (2005) based on 48 European pollen and plant macrofossil records indicate higher summer temperature during the last interglacial (at 125 kyr) compared to the Holocene, associated with higher summer insolation. These data are supported by SST from the Alboran Sea, which show the highest temperatures of the last 130 kyr at ~127–118 kyr (~20–23 °C) (Martrat et al., 2004), while SST from two records in the Iberian Margin show highest temperatures between ~ 128 and 123 kyr (~18–20 °C) and ~126–118 kyr (~19–22 °C) (Pailler and Bard, 2002). As explained above, the enhanced temperature contrast between land and ocean masses due to maxima in summer insolation could have favored humid wind transport from both Mediterranean Sea and North Atlantic Ocean triggering higher fall-winter precipitation at those times. This would agree with climatic interpretations pointing to increasing precipitation under

summer aridity from several previous studies on vegetation changes, isotopic composition and sapropel 5 deposition during the last interglacial period in the Iberian Peninsula, Italy and Greece (Sánchez-Goñi et al., 1999; Tzedakis et al., 2003a; Brauer et al., 2007; Ziegler et al., 2010). Milner et al. (2012) using pollen, macrofossil and mineralogical data, showed that the higher summer insolation and summer warming during the MIS 5e generated a more extreme seasonal moisture than during present and the early Holocene. Moreover, the lowest $\delta^{18}O$ values during the MIS 5e from Soreq Cave also suggest higher rainfall with respect to the Holocene (Bar-Matthews et al., 2003). Abundant precipitation at that time most likely exceeded evapotranspiration in the lake and resulted in positive EAP, triggering higher lake level during the MIS 5e than in other warm periods such as the Holocene or interstadials, resulting in *Carbonate facies* sedimentation instead of *Peat facies*.

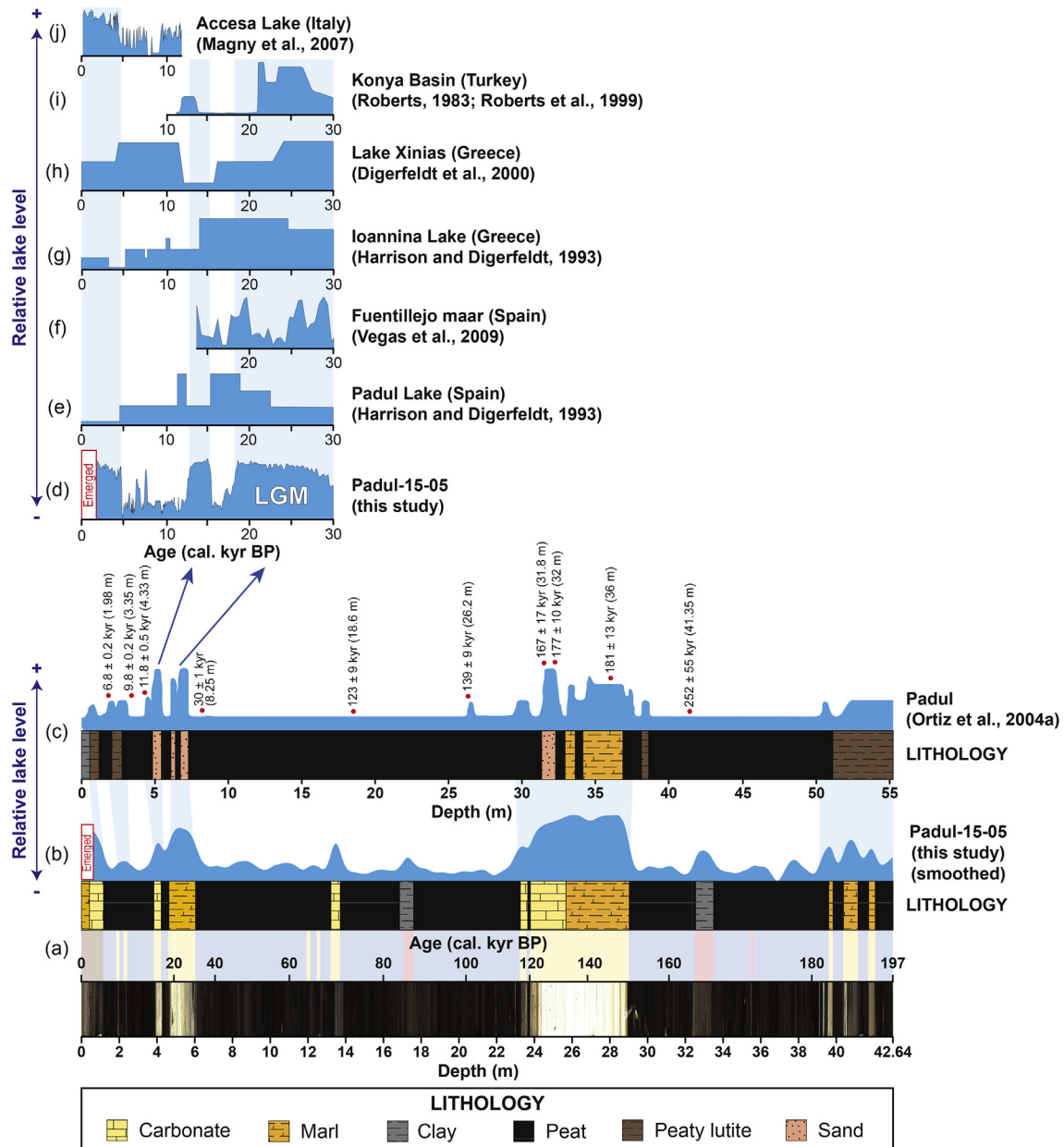### 5.4. Padul and other Mediterranean lake level records

Very few lake level reconstructions from long cores (>100 kyr) exist in the Mediterranean region, being an important parameter to use with other proxies to understand regional climatic changes and the response of local wetland environments. The Padul-15-05 record shows the highest lake levels mainly during the coldest and most arid glacial periods at MIS 6b and 6a and MIS 2 (~155–132 and ~29–18 kyr BP, respectively) and during MIS 5e and the most part of the Younger Dryas/Bølling Allerød (~132–117 kyr and 15.5–12.6 kyr BP, respectively). Previous studies have also shown this apparent contradiction between regional (i.e., pollen) paleoclimate evidence, showing aridity during the last glaciation, and geomorphological evidence for high lake levels in the northern Mediterranean area (Prentice et al., 1992; Harrison and Digerfeldt, 1993; Harrison et al., 1996).

A previous lake level reconstruction from Padul from Ortiz et al. (2004a), based on the organic geochemistry of the core (EQUIP borehole) from Nestares and Torres (1998), shows similar trends with respect to our Padul-15-05 record (Fig. 13). Nevertheless, the age control between our study and the previous work presents discrepancies at ages older than ca. 40 kyr BP. Ortiz et al. (2004a, 2010) indicated the highest lake levels at ~185–170 kyr BP, while our study suggests highest water depth during glacial periods MIS 6a and 6b, and MIS 5e (~155–117 kyr BP), as explained above.

According to the INTIMATE network, the age of the LGM was defined as occurring between 23 and 19 kyr BP (Mix et al., 2001). Tzedakis (2007) summarized that maximum lake levels during the LGM in the eastern Mediterranean region were reached ~27–24 kyr ago, based on different lake level reconstructions from the Dead Sea (Israel, Jordan, Palestine) (Bartov et al., 2002), Lake Kinneret (Israel) (Hazan et al., 2005) and Konya Basin (Turkey) (Roberts, 1983; Roberts et al., 1999). In the central Mediterranean region, different Greek lakes also reached their highest lake levels during the LGM. For example, high lake level in Ioannina occurred ~30–14 kyr ago with the maximum between ~25 and 14 kyr BP (Harrison and Digerfeldt, 1993) while Xinias lake reached its highest level ~30–24 kyr ago, before slightly decreasing until ~16 kyr BP (Digerfeldt et al., 2000) (Fig. 13). In the western Mediterranean, lake level of Padul was reconstructed in a previous study by Harrison and Digerfeldt (1993), who found maximum water depths occurred ~22–15 kyr ago, with the highest values between ~19 and 15 kyr BP. The Fuentillejo maar lake level reconstruction from central Spain (Vegas et al., 2009) also recorded highest lake levels during the glacial period but with a decrease between 24 and 20 kyr BP. In addition, they showed low lake levels between 18 and 15 kyr ago, similar to that recorded in our study from Padul (Fig. 13).

The high lake level reconstruction for the most part of the

Fig. 13. Comparison of different Mediterranean lake level reconstructions. From a to c: (a) scanner photograph of the Padul-15-05 core and lithology with (b) the correspondent lake level reconstruction based on smoothed PC1 data and (c) the correlation with the lake level and lithology from Ortiz et al. (2004a) (plotted with respect to depth). From d to j: comparison of the last 30 kyr lake level reconstructions of (d) Padul-15-05 core from this study, (e) Padul from Harrison and Digerfeldt (1993), (f) Fuentillejo maar from Vegas et al. (2009), (g) Ioannina lake from Harrison and Digerfeldt (1993), (h) lake Xinias from Digerfeldt et al. (2000), (i) Konya basin from Roberts (1983) and Roberts et al. (1999), and (j) lake Accesa from Magny et al. (2007). [14]C ages from Lake Xinias and Konya Basin have been calibrated in order to plot lake level in the same cal. kyr BP scale as the rest of the records.

Younger Dryas/Bølling Allerød (15.5–12.6 kyr BP) in the Padul-15-05 core is similar to the reconstructions from Konya Basin (Turkey) (Roberts, 1983). Our Holocene lake level reconstruction from Padul-15-05 presents similar trends with respect to Ortiz et al. (2004a, 2010), which showed that from 10 kyr to 4.5 kyr BP C_{27}, C_{29} and C_{31} n-alkanes occurred along with vascular plants, macrophytes and high amounts of organic matter, indicative of palustrine conditions and low lake levels (Ortiz et al., 2010). The Accesa Lake (Magny et al., 2007) also presented lower lake level during the early-middle Holocene (~10−5 kyr BP) compared with the last 5000 years BP, in which lake level increased similar to that occurred in Padul-15-05, even if Padul wetland recorded an ephemeral/emerged phase during the last 1500 years, as explained by Ramos-

Roman et al. (2018a). On the contrary, our Holocene reconstruction disagrees with other Mediterranean lake level reconstructions, including the previous reconstructions from Padul (Harrison and Digerfeldt, 1993), Lake Xinias (Digerfeldt et al., 2000) and Ioannina (Harrison and Digerfeldt, 1993), showing higher water depth during early and middle Holocene and a decrease during the late Holocene (Fig. 13). The suggested contrary trend from Harrison and Digerfeldt (1993) at Padul, could be related to lake level interpretations only based on lithological aspects.

Finally, lake level reconstructions for alpine environments from Sierra Nevada (Laguna de Río Seco lake; 3020 m) showed the highest lake levels during the early Holocene (Anderson et al., 2011; Jiménez-Espejo et al., 2014). This contrasts with our lake level

reconstruction from Padul at lower elevation, showing lowest lake levels at that time. This could be explained by the differences in elevation and contrasting precipitation/evapotranspiration balances between the two sites. A greater seasonal insolation difference during the early Holocene may have produced higher snowpack in alpine lakes in Sierra Nevada, in contrast to low elevation areas where high evapotranspiration rates prevailed (Anderson et al., 2011). Therefore, even if regional climate data (i.e., arboreal pollen) pointed into same climatic conditions, lake level could have responded differently depending on the altitude and/or latitude.

6. Conclusions

The high-resolution multiproxy analyses from the new Padul-15-05 sediment record shows:

1. The Padul wetland is confirmed as an extraordinary and unique paleoenvironmental and paleoclimatic site in the Iberian Peninsula, containing one of the few long and continuous sedimentary record (>100 kyr) from the southwestern Europe and Mediterranean region.
2. An improvement of the age-depth model for the Padul sedimentary sequence due to (1) a higher radiocarbon dating resolution for the last ~55 kyr (61 AMS radiocarbon samples), (2) the combination of different and updated dating techniques (AMS radiocarbon dating, specific-compound radiocarbon dating, AAR dating) and (3) the use of the SAR of peat and carbonate/marl lithologies from the well-dated top part of the core, which allowed a more objective estimation of the age control and climate reconstruction of the Padul sedimentary sequence for the last ~197 kyr.
3. Insolation, dominated by orbital-scale precession and to a lesser extent, eccentricity, at this latitude, was the most important factor controlling climatic changes in the Padul area, forcing regional (vegetation) and local (sedimentation, lake level) environmental changes.
4. Lithology/facies representing the local sedimentation were controlled by insolation. High siliciclastic input in the Padul wetland transported from Sierra Nevada mainly occurred during low summer insolation, triggering enhanced arid climate conditions, lower forest cover and higher soil weathering/erosion and/or low biogenic deposition.
5. Lake level variations, reconstructed using statistical analysis from inorganic geochemistry, organic geochemistry and magnetic susceptibility data, were triggered by the precipitation/evapotranspiration balance (EAP). Lake level at Padul, which also controlled lithology/facies sedimentation, showed the highest levels during minima in insolation (cold stadials and glacial periods) and deglaciations, while low water level occurred during warmer interstadials and interglacials (except for MIS 5e). Therefore, cold climate conditions with low evapotranspiration lead to positive EAP and high lake levels (and carbonate/marl precipitation), while high evapotranspiration rates exceeding rainfall during most of the warm periods resulted in negative EAP and low lake levels (and peat sedimentation).
6. The different lithological features, facies and lake levels occurring between the last interglacial and the Holocene interglacial periods are the result of distinct seasonality and temperature/precipitation patterns, driven by different orbital parameters and insolation values. Consequently, during the MIS 5e carbonate lithology predominated due to the positive EAP, in which precipitation exceeded evapotranspiration, in contrast to the period of peat accumulation during the Holocene, characterized by high evapotranspiration rates that exceeded rainfall.
7. Multiproxy analysis of sedimentary sequences, including statistical data processing, is necessary to produce a more comprehensive picture of the environmental and climatic changes affecting the local and regional environments in a wetland area.

Appendix A. Supplementary data

Supplementary data related to this article can be found at https://doi.org/10.1016/j.quascirev.2018.08.014.

References

Allen, J.R.M., Brandt, U., Brauer, A., Hubberten, H.W., Huntley, B., Keller, J., Kraml, M., Mackensen, A., Mingram, J., Negendank, J.F.W., Nowaczyk, N.R., Oberhänsli, H., Watts, W.A., Wulf, S., Zolitschka, B., 1999. Rapid environmental changes in southern Europe during the last glacial period. Nature 400, 740–743.

Allen, J.R.M., Watts, W.A., Huntley, B., 2000. Weichselian palynostratigraphy, palaeovegetation and palaeoenvironment; the record from Lago Grande di Monticchio, southern Italy. Quat. Int. 73/74, 91–110.

Alonso-Zarza, A.M., Calvo, J.P., García del Cura, M.A., 1992. Palustrine sedimentation and associated features — grainification and pseudo-microkarst — in the middle Miocene (intermediate unit) of the madrid basin, Spain. Sediment. Geol. 76, 43–61.

Anderson, R.S., Jiménez-Moreno, G., Carrión, J.S., Pérez-Martínez, C., 2011. Postglacial history of alpine vegetation, fire, and climate from Laguna de Río Seco, Sierra Nevada, southern Spain. Quat. Sci. Rev. 30, 1615–1629.

Aranbarri, J., González-Sampériz, P., Valero-Garcés, B., Moreno, A., Gil-Romera, G., Sevilla-Callejo, M., García-Prieto, E., Di Rita, F., Mata, M.P., Morellón, M., Magri, D., Rodríguez-Lázaro, J., Carrión, J.S., 2014. Rapid climatic changes and resilient vegetation during the Lateglacial and Holocene in a continental region of south-western Europe. Global Planet. Change 114, 50–65.

Bahr, A., Jiménez-Espejo, F.J., Kolasinac, N., Grunert, P., Hernández-Molina, F.J., Röhl, U., Voelker, A.H.L., Escutia, C., Stow, D.A.V., Hodell, D., Alvarez-Zarikian, C.A., 2014. Deciphering bottom current velocity and paleoclimate signals form contourite deposits in the Gulf of Cádiz during the last 140 kyr: an inorganic geochemical approach. G-cubed 15, 3145–3160.

Bar-Matthews, M., Ayalon, A., Gilmour, M., Matthews, A., Hawkesworth, C.J., 2003. Sea-land oxygen isotopic relationships from planktonic foraminifera and speleothems in the Eastern Mediterranean region and their implication for paleorainfall during interglacial intervals. Geochimica et Cosmochimica Acta 67 (17), 3181–3199.

Barker, S., Knorr, G., Edwards, L., Parrenin, F., Putnam, A.E., Skinner, L.C., Wolff, E., Ziegler, M., 2011. 800,000 years of abrupt climate variability. Science 334, 347–351.

Bartov, Y., Stein, M., Enzel, Agnon, A., Reches, Z., 2002. lake levels and sequence stratigraphy on lake lisan, the late Pleistocene precursor of the Dead Sea. Quat. Res. 57, 9–21.

Beas, J., 1990. Acuífero del borde oeste de Sierra Nevada: Sierra del Padul-La Peza. Atlas hidrogeológico de la provincia de Granada. Instituto Tecnológico Geominero de España y Diputación Provincial de Granada.

Berger, A., Loutre, M.F., Mélice, J.L., 1998. Instability of the astronomical periods from 1.5 Myr BP to 0.5 Myr AP. Paleoclimates 2 (4), 239–280.

Berger, A., Loutre, M.F., Kaspar, F., Lorenz, S.J., 2007. Chapter 2: insolation during interglacial. In: Developments in Quaternary Sciences, vol. 7, pp. 13–27.

Bertini, A., 2001. Pliocene climatic cycles and altitudinal forest development from 2.7 Ma in the northern Apennines (Italy): evidences from the pollen record of the Stirone section (~ 5.1 to 2.2 Ma). Geobios 34, 253–265.

Blaauw, M., 2010. Methods and code for "classical" age-modelling of radiocarbon sequences. Quat. Geochronol. 5, 512–518.

Blaauw, M., 2012. Out of tune: the dangers of aligning proxy archives. Quat. Sci. Rev. 36, 38–49.

Brauer, A., Allen, J.R.M., Mingram, J., Dulski, P., Wulf, S., Huntley, B., 2007. Evidences for last interglacial chronology and environmental change from Southern Europe. Proc. Natl. Acad. Sci. Unit. States Am. 104 (2), 450–455.

Buurman, P., 1980. Paleosols in the reading beds (Palaeocene) of Alum bay, isle of Wight, UK. Sedimentology 27, 593–606.

Carrasco Duarte, M., 1998. El Padul, 389 pp.

Castillo Martín, A., 2009. Lagunas de Sierra Nevada. Editorial Universidad de Granada, Granada.

Castillo Martín, A., Fernández-Rubio, R., 1984. Hidrogeología de la cuenca vertiente a la depresión de Padul (Granada). I Congreso Español de Geología. Tomo IV, pp. 109–121.

Cohen, A.S., 2003. Paleolimnology: the History and Evolution of Lake Systems. Oxford University Press, New York.

Combourieu-Nebout, N., 1993. Vegetation response to Upper Pliocene glacial/interglacial cyclicity in the central Mediterranean. Quat. Res. 40, 228–236.

Combourieu-Nebout, N., Turon, J.L., Capotondi, L., Londeix, L., Pahnke, K., 2002. Enhanced aridity and atmospheric high-pressure stability over the western Mediterranean during the North Atlantic cold events of the past 50 k. y. Geology 30 (10), 863–866.

Corzo, A.,A., Luzón, A., Mayayo, van Bergeijk, M.J., Mata, P., García de Lomas, J., 2005. Carbonate mineralogy along a biogeochemical gradient in recent lacustrine sediments of Gallocanta Lake (Spain). Geomicrobiol. J. 22, 283–298.

Deines, P., 1980. The isotopic composition of reduced organic carbon. In: Fritz, F., Fontes, J.C. (Eds.), Handbook of Environmental Isotope Geochemistry, vol. 1. The terrestrial environment, pp. 329–406.

Delgado, J., Alfaro, P., Galindo-Zaldívar, J., Jabaloy, A., López Garrido, A.C., Sanz de Galdeano, C., 2002. Structure of the Padul-Nigüelas Basin (S Spain) from H/V ratios of ambient noise: application of the method to study peat and coarse sediments. Pure Appl. Geophys. 159, 2733–2749.

Develle, A.L., Gasse, F., Vidal, L., Williamson, D., Demory, F., Van Campo, E., Ghaleb, B., Thouveny, N., 2011. A 250 ka sedimentary record from a small karstic lake in the Northern Levant (Yammoûneh, Lebanon): paleoclimatic implications. Palaeogeogr. Palaeoclimatol. Palaeoecol. 305, 10–27.

Digerfeldt, G., Olsson, S., Sandgren, P., 2000. Reconstruction of lake-level changes in lake Xinias, central Greece, during the last 40000 years. Palaeogeogr. Palaeoclimatol. Palaeoecol. 158, 65–82.

Domingo-García, M., Fernández-Rubio, R., López-González, J.D., González-Gómez, C., 1983. Aportación al conocimiento de la neotectónica de la depresión de Padul (Granada). Revista española de geología y minería 53, 6–16.

El Aallali, A., Nieto, J.M.L., Raya, F.A.P., Mesa, J.M., 1998. Estudio de la vegetación forestal en la vertiente sur de Sierra Nevada (Alpujarra Alta granadina). Itinera Geobot. 11, 387–402.

Ertel, J.R., Hedges, J.I., 1985. Sources of sedimentary humic substances: vascular plant debris. Geochem. Cosmochim. Acta 49, 2097–2107.

Faegri, K., Iversen, J., 1989. Textbook of Pollen Analysis. Wiley, New York.

Fernández, S., Fuentes, N., Carrión, J.S., González-Sampériz, P., Montoya, E., Gil, G., Vega-Toscano, G., Riquelme, J.A., 2007. The Holocene and upper Pleistocene pollen sequence of Carihuela cave, southern Spain. Geobios 40, 75–90.

Ficken, K.J., Li, B., Swain, D.L., Eglinton, G., 2000. An n-alkane proxy for the sedimentary input of submerged/floating freshwater aquatic macrophytes. Org. Geochem. 31, 745–749.

Fletcher, W.J., Sánchez-Goñi, M.F., 2008. Orbital- and sub-orbital-scale climate impacts on vegetation of the western Mediterranean basin over the last 48,000 yr. Quat. Res. 70, 451–464.

Fletcher, W., Sánchez-Goñi, M.F., Allen, J.R.M., Cheddadi, R., Combourieu-Nebout, N., Huntley, B., Lawson, I., Londeix, L., Magri, D., Margari, V., Müller, U.C., Naughton, F., Novenko, E., Roucoux, K., Tzedakis, P.C., 2010. Millennial-scale variability during the last glacial in vegetation records from Europe. Quat. Sci. Rev. 29, 2839–2864.

Florschütz, F., Menéndez-Amor, J., Wijmstra, T.A., 1971. Palynology of a thick Quaternary succession in southern Spain. Palaeogeogr. Palaeoclimatol. Palaeoecol. 10, 233–264.

Francke, A., Wagner, B., Just, J., Leicher, N., Gromig, R., Baumgarten, H., Vogel, H., Lacey, J.H., Sadori, L., Wonik, T., Leng, M.J., Zanchetta, G., Sulpizio, R., Giaccio, B., 2016. Sedimentological processes and environmental variability at Lake Ohrid (Macedonia, Albania) between 637 ka and the present. Biogeosciences 13, 1179–1196.

García-Prieto, E., 2015. Dinámica paleoambiental durante los últimos 135.000 años en el Alto Jiloca: el registro lacustre de El Cañizar. Tesis doctoral. Universidad de Zaragoza.

Gómez Ortiz, A., Schulte, L., Salvador Franch, F., Palacios Estremera, D., Sanz de Galdeano, C., Sanjosé Blasco, J.J., Tanarro García, L.M., Atkinson, A., 2005. The Geomorphological unity of the Veleta: a Particular Area of the Sierra Nevada Guidebook. Sixth International Conference of Geomorphology, Zaragoza.

González-Donoso, J.M., Galleo, J.A., Sánz de Galdeano, C., 1978. Hoja Geológica MAGNA Núm, 1026 (Padul), escala 1:50.000. Instituto Geológico y Minera de España.

González-Sampériz, P., García-Prieto, E., Aranbarri, J., Valero-Garcés, B.L., Moreno, A., Gil-Romera, G., Sevilla-Callejo, M., Santos, L., Morellón, M., Mata, P., Andrade, A., Carrión, J.S., 2013. Reconstrucción paleoambiental del último ciclo glacial-interglacial en la Iberia continental: la secuencia del cañizar de Villarquemado (Teruel). Cuadernos de Investigación Geográfica 39 (1), 49–76.

González-Sampériz, P., Aranbarri, J., Pérez-Sanz, A., Gil-Romera, G., Moreno, A., Leunda, M., Sevilla-Callejo, M., Corella, J.P., Morellón, M., Oliva, B., Valero-Garcés, B., 2017. Environmental and climate change in the southern Central Pyrenees since the Last Glacial Maximum: a view from the lake records. Catena 149, 668–688.

Hammer, Ø., Harper, D.A.T., Ryan, P.D., 2001. PAST: paleontological Statistics software package for Education and data analysis. Available at: http://folk.uio.no/ohammer/past/.

Harrison, S.P., Digerfeldt, G., 1993. European lakes as palaeohydrological and palaeoclimatic indicators. Quat. Sci. Rev. 12, 233–248.

Harrison, S.P., Yu, G., Tarasov, P.E., 1996. Late Quaternary lake-level record from northern Eurasia. Quat. Res. 45, 138–159.

Harvey, A.M., Wigand, P.E., Wells, S.G., 1999. Response of alluvial fan system to the late Pleistocene to Holocene climatic transition: contrast between the margins of pluvial Lakes Lahontan and Mojave, Nevada and California, USA. Catena 36, 255–281.

Hazan, N., Stein, M., Agnon, A., Marco, S., Nadel, D., Negendank, J.F.W., Schwab, M.J., Neev, D., 2005. The late Quaternary limnological history of Lake Kinneret (sea of Galilee), Israel. Quat. Res. 63, 60–77.

Hodge, E.J., Richards, D.A., Smart, P.L., Andreo, B., Hoffmann, D.L., Mattey, D.P., González-Ramón, A., 2008. Effective precipitation in southern Spain (~ 266 to 46 ka) based on a speleothem stable carbon isotope record. Quat. Res. 69, 447–457.

Imbrie, J., Imbrie, J.Z., 1980. Modeling the climatic response to orbital variations. Science 207, 943–953.

Jiménez-Espejo, F.J., García-Alix, A., Jiménez-Moreno, G., Rodrigo-Gámiz, M., Anderson, R.S., Rodríguez-Tovar, F.J., Martínez-Ruiz, F., Giralt, S., Delgado Huertas, A., Pardo-Igúzquiza, E., 2014. Saharan aeolian input and effective humidity variations over western Europe during the Holocene from a high altitude record. Chem. Geol. 374–375, 1–12.

Jiménez-Moreno, G., García-Alix, A., Hernández-Corbalán, M.D., Anderson, R.S., Delgados-Huertas, A., 2013. Vegetation, fire, climate and human disturbance history in the southwestern Mediterranean area during the late Holocene. Quat. Res. 79, 110–122.

Jones, B., Renaut, R.W., 2010. Chapter 4: calcareous spring deposits in continental settings. In: Alonso-Zarza, A.M., Tanner, L.H. (Eds.), Carbonate in Continental Settings: Facies, Environments and Processes, vol. 61. Development in Sedimentology, pp. 177–224.

Kaspar, F., Kühl, N., Cubasch, U., Litt, T., 2005. A model-data comparison of European temperatures in the Eemian interglacial. Geophys. Res. Lett. 32, L11703.

Kaufman, D.S., Manley, W.F., 1998. A new procedure for determination of DL amino acid ratios in fossils using reverse phase liquid chromatography. Quat. Sci. Rev. 17, 987–1000.

Kutzbach, J.E., Guetter, P.J., 1986. The influence of changing orbital parameters and surface boundary conditions on climate simulations for the past 18000 years. J. Atmos. Sci. 43 (16), 1726–1759.

Laabs, B.J.C., Kaufman, D.S., 2003. Quaternary highstands in bear lake valley, Utah and Idaho. Geol. Soc. Am. Bull. 115, 463–478.

Lionello, P., Sanna, A., 2005. Mediterranean wave climate variability and its links with NAO and Indian Monsoon. Clim. Dynam. 25, 611–623.

Litt, T., Pickarski, N., Heumann, G., Stockhecke, M., Tzedakis, P.C., 2014. A 600,000 years long continental pollen record from Lake Van, eastern Anatolia (Turkey). Quat. Sci. Rev. 104, 30–41.

Magny, M., de Beaulieu, J.L., Drescher-Schneider, R., Vannière, B., Walter-Simonnet, A.V., Miras, Y., Millet, L., Bossuet, G., Peyron, O., Brugiapaglia, E., Leroux, A., 2007. Holocene climate changes in the central Mediterranean as recorded by lake-level fluctuations at Lake Accesa (Tuscany, Italy). Quat. Sci. Rev. 26, 1736–1758.

Martin, J.D., 2004. Using XPowder: a Software Package for Powder X-Ray Diffraction Analysis. Legal Deposit GR, 1001/04. Available at: www.xpowder.com.

Martrat, B., Grimalt, J.O., Lopez-Martinez, C., Cacho, I., Sierro, F.J., Flores, J.A., Zahn, R., Canals, M., Curtis, J.H., Hodell, D.A., 2004. Abrupt temperature changes in the western Mediterranean over the past 250,000 years. Science 306, 1762–1765.

Members, C.O.H.M.A.P., 1988. Climatic changes of the last 18,000 years, observations and model simulations. Science 242, 1043–1052.

Menéndez-Amor, J., Florschütz, F., 1962. Un aspect de la végétation en Espagne méridionale durant la dernière glaciation et L'Holocène. Geol. Mijnbouw 131–134.

Menéndez-Amor, J., Florschütz, F., 1964. Results of the preliminary palynological investigation of samples from a 50 m boring in southern Spain. Bol. R. Soc.

Española His. Nat. 62, 251–255.

Meyers, P.A., 1994. Preservation of elemental and isotopic source identification of sedimentary organic matter. Chem. Geol. 144, 289–302.

Milankovitch, M., 1920. Théorie mathématique des phénomènes thermiques produits par la radiation solaire. Royal Serb. Acad., Spec. Publi. 133, 1–633.

Milner, A.M., Collier, R.E.L., Roucoux, K.H., Müller, U.C., Pross, J., Kalaitzidis, S., Christanis, K., Tzedakis, P., 2012. Enhanced seasonality of precipitation in the Mediterranean during the early part of the Last Interglacial. Geology 40 (10), 919–922.

Milner, A.M., Roucoux, K.H., Collier, R.E.L., Müller, U.C., Pross, J., Tzedakis, P.C., 2016. Vegetation responses to abrupt climatic changes during the last interglacial complex (marine isotope stage 5) at Tenaghi Philippon, NE Greece. Quat. Sci. Rev. 154, 169–181.

Mitterer, R.M., Kriausakul, N., 1989. Calculation of amino acid racemiation ages based on apparent parabolic kinetics. Quat. Sci. Rev. 8, 353–357.

Mix, A.C., Bard, E., Schneider, R., 2001. Environmental processes of the ice age: land, oceans and glaciers (EPILOG). Quat. Sci. Rev. 20, 627–657.

Morellón, M., Aranbarri, J., Moreno, A., González-Sampériz, P., Valero-Garcés, B.L., 2018. Early Holocene humidity patterns in the Iberian Peninsula reconstructed from lake, pollen and speleothem records. Quat. Sci. Rev. 181, 1–18.

Moreno, A., González-Sampériz, P., Morellón, M., Valero-Garcés, B.L., Fletcher, W.J., 2012. Northern Iberian abrupt climate change dynamics during the last glacial cycle: a view from lacustrine sediments. Quat. Sci. Rev. 36, 139–153.

Nelson, D.W., Sommers, L.E., 1982. Total carbon, organic carbon, and organic matter. In: Methods of Soil Analysis, Part 2. America Society of Agronomy, Madison, Wisconsin, USA, pp. 539–579.

Nestares, T., Torres, T., 1998. Un nuevo sondeo de investigación paleoambiental del Pleistoceno y Holoceno en la turbera de Padul (Granada, Andalucía). Geogaceta 23, 99–102.

North Greenland Ice Core Project members (NGRIP-Members), 2004. High-resolution record of Northern Hemisphere climate extending into the last interglacial period. Nature 431 (7005), 147–151.

Ortiz, J.E., Torres, T., Delgado, A., Juliá, R., Lucini, M., Llamas, F.J., Resyes, E., Soler, V., Valle, M., 2004a. The palaeoenvironmental and palaeohydrological evolution of Padul Peat Bog (Granada, Spain) over one million years, from elemental, isotopic and molecular geochemical proxies. Org. Geochem. 35, 1243–1260.

Ortiz, J.E., Torres, T., Julià, R., Delgado, A., Llamas, F.J., Soler, V., Delgado, J., 2004b. Numerical dating algorithms of amino acid racemization ratios from continental ostracods. Application to the Guadix-Baza Basin (southern Spain). Quat. Sci. Rev. 23, 717–730.

Ortiz, J.E., Torres, T., Delgado, A., Llamas, J.F., Soler, V., Valle, M., Juliá, R., Moreno, L., Díaz-Bautista, A., 2010. Palaeoenvironmental changes in the Padul basin (Granada, Spain) over the last 1 Ma based on the biomarker content. Palaeogeogr. Palaeoclimatol. Palaeoecol. 298, 286–299.

Ortiz, J.E., Moreno, L., Torres, T., Vegas, J., Ruiz-Zapata, B., García-Cortés, A., Galán, L., Pérez-González, A., 2013. A 220 ka palaeoenvironmental reconstruction of the Fuentillejo maar lake record (Central Spain) using biomarker analysis. Org. Geochem. 55, 85–97.

Paillard, D., Labeyrie, L., Yiou, P., 1996. Macintosh Program performs time-series analysis. Eos Trans. Am. Geophys. Union 77, 379.

Pailler, D., Bard, E., 2002. High frequency palaeoceanographic changes during the past 140000 yr recorded by the organic matter in sediments of the Iberian Margin. Palaeogeogr. Palaeoclimatol. Palaeoecol. 181, 431–452.

Palacios, D., Gómez-Ortiz, A., Andrés, N., Salvador, F., Oliva, M., 2016. Timing and new geomorphologic evidence of the last deglaciation stages in Sierra Nevada (southern Spain). Quat. Sci. Rev. 150, 110–129.

Pelechaty, M., Pukacz, A., Apolinarska, K., Pelechata, A., Siepak, M., 2013. The significance of *Chara* vegetation in the precipitation of lacustrine calcium carbonate. Sedimentology 60 (4), 1017–1035.

Pentecost, A., 2005. Travertine. Springer, Berlin, p. 445.

Pérez Raya, F., López Nieto, J.M., 1991. Vegetación acuática y helofítica de la depresión de Padul (Granada). Acta Bot. Malacitana 16 (2), 373–389.

Pons, A., Reille, M., 1988. The Holocene- and upper Pleistocene pollen record from Padul (Granada, Spain): a new study. Palaeogeogr. Palaeoclimatol. Palaeoecol. 66, 243–263.

Prentice, I.C., Guiot, J., Harrison, S.P., 1992. Mediterranean vegetation, lake levels and palaeoclimate at the Last Glacial Maximum. Nature 360, 658–660.

Pross, J., Koutsodendris, A., Christanis, K., Fischer, T., Fletcher, W.J., Hardiman, M., Kalaitzidis, S., Knipping, M., Kotthoff, U., Milner, A.M., Müller, U.C., Schmiedl, G., Siavalas, G., Tzedakis, P.C., Wulf, S., 2015. The 1.35-Ma-long terrestrial climate archive of Tenaghi Philippon, northeastern Greece: evolution, exploration, and perspectives for future research. Newsl. Stratigr. 48 (3), 253–276.

Ramos-Román, M.J., 2018. Holocene Paleoenvironmental Change, Climate and Human Impact in Sierra Nevada, Southern Iberian Peninsula. PhD Thesis. University of Granada.

Ramos-Román, M.J., Jiménez-Moreno, G., Camuera, J., García-Alix, A., Anderson, R.S., Jiménez-Espejo, F.J., Carrión, J.S., 2018a. Holocene climate aridification trend and human impact interrupted by millennial- and centennial-scale climate fluctuations from a new sedimentary record from Padul (Sierra Nevada, southern Iberian Peninsula). Clim. Past 14, 117–137.

Ramos-Román, M.J., Jiménez-Moreno, G., Camuera, J., García-Alix, A., Anderson, R.S., Jiménez-Espejo, F.J., Sachse, D., Toney, J.L., Carrión, J.S., Webster, C., Yanes, Y., 2018b. Millennial-scale cyclical environment and climate variability during the Holocene in the western Mediterranean region deduced from a new multi-proxy analysis from the Padul record (Sierra Nevada, Spain). Global Planet.

Change 168, 35–53.

Reimer, P.J., Bard, E., Bayliss, A., Beck, J.W., Blackwell, P.G., Ramsey, C.B., Buck, C.E., Cheng, H., Edwards, R.L., Friedrich, M., Grootes, P.M., Guilderson, T.P., Haflidason, H., Hajdas, I., Hatté, C., Heaton, T.J., Hoffmann, D.L., Hogg, A.G., Hughen, K.A., Kaiser, K.F., Kromer, B., Manning, S.W., Niu, M., Reimer, R.W., Richards, D.A., Scott, E.M., Southon, J.R., Staff, R.A., Turney, C.S.M., van der Plicht, J., 2013. Intcal13 and Marine13 radiocarbon age calibration curves 0-50,000 years cal BP. Radiocarbon 55 (4), 1869–1887.

Roberts, N., 1983. Age, palaeoenvironmental, and climatic significance of late Pleistocene Konya lake, Turkey. Quat. Res. 19, 154–171.

Roberts, N., Black, S., Boyer, P., Eastwood, W.J., Griffiths, H.I., Lamb, H.F., Leng, M.J., Parish, R., Reed, J.M., Twigg, D., Yigitbasioglu, H., 1999. Chronology and stratigraphy of late Quaternary sediments in the Konya basin, Turkey: results from the KOPAL project. Quat. Sci. Rev. 18, 611–630.

Rodó, X., Baert, E., Comin, F.A., 1997. Variations in seasonal rainfall in southern Europe during the present century: relationship with the north Atlantic oscillation and El Niño-southern oscillation. Clim. Dynam. 13, 275–284.

Sánchez-Goñi, M.F., Eynaud, F., Turon, J.L., Shackleton, N.J., 1999. High resolution palynological record off the Iberian margin: direct land-sea correlation for the Last Interglacial complex. Earth Planet Sci. Lett. 171, 123–137.

Santanach, P.F., Sanz de Galdeano, C., Bousquet, J.C., 1980. Neotectónica de las regiones mediterráneas de España (Cataluña y Cordilleras Béticas). Boletín Geológico y Minero, pp. 417–440. T. XCI-II.

Satow, C.G., 2012. The Tephrostratigraphy of Three, Late Quaternary, Mediterranean marine Cores. PhD Thesis. University of London.

Schulte, L., 2002. Climatic and human influence on river systems and glacier fluctuations in southeast Spain since the Last Glacial Maximum. Quat. Int. 93–94, 85–100.

Schulz, M., Mudelsee, M., 2002. REDFIT: estimating red-noise spectra directly from unevenly spaced paleoclimatic time series. Comput. Geosci. 28, 421–426.

Sierralta, M., Urban, B., Linke, G., Frechen, M., 2017. Middel Pelistocene interglacial peat deposits from Northern Germany investigated by 230 Th/U and palynology: case studies from Wedel and Schöningen. Zeitschrift der Dtsch. Gesellschaft für Geowissenchaften 168, 373–387.

Sun, Y., An, Z., 2005. Late Pliocene-Pleistocene changes in mass accumulation rates of eolian deposits on the central Chinese Loess Plateau. J. Geophys. Res. 110, 1–8.

Turner, C., West, R.G., 1968. The subdivision and zonation of interglacial periods. Eiszeitalt. Ggw. 19, 93–101.

Tzedakis, P.C., 2007. Seven ambiguities in the Mediterranean palaeoenvironmental narrative. Quat. Sci. Rev. 26, 2042–2066.

Tzedakis, P.C., Lawson, I.T., Frogley, M.R., Hewitt, G.M., Preece, R.C., 2002. Buffered tree population changes in a Quaternary refugium: evolutionary implications. Science 297, 2044–2047.

Tzedakis, P.C., Frogley, M.R., Heaton, T.H.E., 2003a. Last Interglacial conditions in southern Europe: evidence from Ioannina, northwest Greece. Global Planet. Change 36, 157–170.

Tzedakis, P.C., McManus, J.F., Hooghiemstra, H., Oppo, D.W., Wijmstra, T.A., 2003b. Comparison of changes in vegetation in northeast Greece with records of climate variability on the orbital and suborbital frequencies over the last 450000 years. Earth Planet Sci. Lett. 212, 197–212.

Tzedakis, P.C., Hooghiemstra, J.F., Pälike, H., 2006. The last 1.35 million years at Tenaghi Philippon: revised chronostratigraphy and long-term vegetation trends. Quat. Sci. Rev. 25, 3416–3430.

Vaks, A., Bar-Matthews, M., Ayalon, A., Schilman, B., Gilmour, M., Hawkesworth, C.J., Frumkin, A., Kaufman, A., Matthews, A., 2003. Paleoclimate reconstruction based on the timing of speleothem growth and oxygen and carbon isotope composition in a cave located in the rain shadow in Israel. Quat. Res. 59, 182–193.

Valero-Garcés, B.L., Zeroual, E., Kelts, K., 1998. Arid phases in the western Mediterranean region during the Last Glacial Cycle reconstructed from lacustrine records. Paleohydrology and Environmental Change 76–80.

Valle, F., 2003. Mapa de series de vegetación de Andalucía. Editorial Rueda, S.l., Madrid.

Vegas, J., Ruiz-Zapata, B., Ortiz, J.E., Galán, L., Torres, T., García-Cortés, A., Gil-García, M.J., Pérez-González, A., Gallardo-Millán, J.L., 2009. Identification of arid phases during the last 40 cal. ka BP from the Fuentillejo maar-lacustrine record (Campo de Calatrava Volcanic Field, Spain). J. Quat. Sci. 25 (7), 1051–1062.

Wagner, B., Wilke, T., Krastel, S., Zanchetta, G., Sulpizio, R., Reicherter, K., Leng, M., Grazhdani, A., Trajanovski, S., Levkov, Z., Reed, J., Wonik, T., 2014. More than one million years of history in Lake Ohrid cores. Eos 95 (3), 25–32.

Wagner, B., Wilke, T., Francke, A., Albrecht, C., Baumgarten, H., Bertini, A., Combourieu-Nebout, N., Cvetkoska, A., D'Addabbo, M., Donders, T., Föller, K., Giaccio, B., Grazhdani, A., Hauffe, T., Holtvoeth, J., Joannin, S., Jovanovska, E., Just, J., Kouli, K., Koutsodendris, A., Krastel, S., Lacey, J.H., Leicher, N., Leng, M.J., Levkov, Z., Lindhorst, K., Masi, A., Mercuri, A.M., Nomade, S., Nowaczyk, N., Panagiotopoulos, K., Peyron, O., Reed, J.M., Regattieri, E., Sadori, L., Sagnotti, L., Stelbrink, B., Sulpizio, R., Tofilovska, S., Torri, P., Vogel, H., Wagner, B., Wagner-Cremer, F., Wolff, G.A., Wonik, T., Zanchetta, G., Zhang, X.S., 2017. The environmental and evolutionary history of Lake Ohrid (FYROM/Albania): interim results from the SCOPSCO deep drilling project. Biogeosciences 14, 2033–2054.

Watts, W.A., Allen, J.R.M., Huntley, B., 1996. Vegetation history and palaeoclimate of the last glacial period at Lago Grande di Monticchio, southern Italy. Quat. Sci. Rev. 15, 133–153.

Wells, N.A., 1983. Carbonate deposition, physical limnology and environmentally.controlled chert formation in Paleocene-Eocene Lake Flagstaff, Central

Utah. Sediment. Geol. 35, 263—296.

Wijmstra, T.A., 1969. Palynology of the first 30 meters of a 120 m deep section in northern Greece. Acta Bot. Neerl. 18 (4), 511—527.

Wright, 1999. The role of sulphate-reducing bacteria and cyanobacteria in dolomite formation in distal ephemeral lakes of the Coorong region, South Australia. Sediment. Geol. 126, 147—157.

Yamame, M., Yokoyama, Y., Miyairi, Y., Suga, H., Matsuzaki, H., Dunbar, R.B., Ohkouchi, N., 2014. Compound-specific ^{14}C dating of IODP expedition 318 core

U1357A obtained off the Wilkes Land coast, Antarctica. Radiocarbon 56 (4), 1—9.

Yokoyama, Y., Koizumi, M., Matsuzaki, H., Miyairi, Y., Ohkouchi, N., 2010. Developing ultra small-scale radiocarbon sample measurement at the University of Tokyo. Radiocarbon 52 (2), 310—318.

Ziegler, M., Tuenter, E., Lourens, L.J., 2010. The precession phase of the boreal summer monsoon as viewed from the eastern Mediterranean (ODP Site 968). Quat. Sci. Rev. 29, 1481—1490.